5-2004

Time-Resolved Measurements of Plasma Electron Number Density and Electron-Neutral Collision Frequency Using a Microwave Diagnostic Method

Yunqiang Yang
University of Tennessee - Knoxville

To the Graduate Council:

I am submitting herewith a thesis written by Yunqiang Yang entitled "Time-Resolved Measurements of Plasma Electron Number Density and Electron-Neutral Collision Frequency Using a Microwave Diagnostic Method." I have examined the final electronic copy of this thesis for form and content and recommend that it be accepted in partial fulfillment of the requirements for the degree of Master of Science, with a major in Electrical Engineering.

M. Mostofa Howlader, Major Professor

We have read this thesis and recommend its acceptance:

J. Reece Roth, Marshall O. Pace

Accepted for the Council:
Dixie L. Thompson

Vice Provost and Dean of the Graduate School

(Original signatures are on file with official student records.)

To the Graduate Council:

I am submitting herewith a thesis written by Yunqiang Yang entitled "Time-Resolved Measurements of Plasma Electron Number Density and Electron-Neutral Collision Frequency Using a Microwave Diagnostic Method." I have examined the final electronic copy of this thesis for form and content and recommend that it be accepted in partial fulfillment of the requirements for the degree of Master of Science, with a major in Electrical Engineering.

M. Mostofa Howlader
Major Professor

We have read this thesis
and recommend its acceptance:

J. Reece Roth

Marshall O. Pace

Accepted for the Council:

Anne Mayhew
Vice Chancellor and Dean of Graduate Studies

(Original signatures are on file with official student records)

Time-Resolved Measurements of Plasma Electron Number Density and Electron-Neutral Collision Frequency Using a Microwave Diagnostic Method

A Thesis Presented for the
Master of Science Degree
The University of Tennessee, Knoxville

Yunqiang Yang
May 2004

ACKNOWLEDGEMENTS

There are several people to whom I am grateful for enriching my educational experience at the University of Tennessee. I would like to thank my advisor, Professor M. Mostofa Howlader, for his encouragement and guidance in attaining my educational goals. I have benefited greatly from the educational and research instruction of Professor J. Reece Roth, whose ideas will shape my thoughts for years to come. I would also like to express my appreciation to my Thesis Committee, Professor M. Mostofa Howlader, Professor J. Reece Roth, and Professor Marshall O. Pace, for their support and comments.

There are a number of people whose assistance should be recognized. I would like to thank Dr. Jozef Rahel and Mr. Zhiyu Chen for their comments and help for my study.

Lastly, this work is supported in part by AFOSR Contract AF F49620-01-1-0425, and by a subcontract with Atmospheric Glow Technologies LLC under AFOSR Topic AF02-TO13.

ABSTRACT

Microwave interferometry is an established non-perturbing plasma diagnostic technique. Compared with other diagnostic techniques, it can be more robust and reliable in experimental applications. This thesis studies a simple and accurate microwave diagnostic method to characterize the electron number density and electron-neutral collision frequency, which are crucial to understanding the behavior and transport coefficients of plasma. This method is based on a modern vector network analyzer and measures the attenuation and phase shift of a microwave signal when propagating through a plasma layer. These measured quantities are related to the real and imaginary parts of the plasma index of refraction, which is described by Appleton's equation and characterized by plasma parameters, including the electron number density and collision frequency. One can numerically derive these plasma parameters from the measured quantities by using Appleton's equation. Since the electron number density and collision frequency can be calculated from measured quantities, one need not know the electron energy distribution function, the electron kinetic temperature, or the electron energy-dependent cross section for the collision process.

The experimental measurements focus on the time-averaged and time resolved parameters of commercial fluorescent lamp plasma and the One Atmosphere Uniform Glow Discharge Plasma (OAUGDP^{TM}). The latter is an atmospheric pressure glow discharge developed at the UT Plasma Sciences Lab. Since the plasma properties should be periodic with the applied plasma driving frequency, 60 Hz for fluorescent lamp plasma and 2-10 KHz for OAUGDP^{TM} plasma, time-resolved measurements are taken to exhibit the variation of electron number density and collision frequency during one 60 Hz cycle of the fluorescent lamp plasma. This time-resolved measurement is achieved by applying the external trigger feature of the network analyzer.

TABLE OF CONTENTS

Chpater 1. Introduction **1**

Chapter 2. Theory of Microwave-Plasma Interaction **4**

2.1 Definition of Plasma Parameters *4*

2.2 Two EM-Plasma Interaction Modes *5*

2.3 EM Wave Propagating in Particle Interaction Regime *6*

2.4 Attenuation and Phase Shift *6*

Chapter 3. Operation of the Network Analyzer System **12**

3.1 HP 8510C Vector Network Analyzer *12*

3.2 Time Domain Measurement *16*

3.3 External Triggering *20*

Chapter 4. Measurement of a Fluorescent Lamp Plasma **23**

4.1 Fluorescent Lamp *23*

4.2 Measurement System *25*

4.3 Time-Resolved Measurement Configuration *28*

4.4 Measured and Calculated Results *32*

Chapter 5. Measurements of a OAUGDP^{TM} Plasma **39**

5.1 Atmospheric Pressure Plasma Diagnostics *39*

5.2 Measurement of a Surface OAUGDP^{TM} Generated by a Flat Panel *41*

5.3 Investigation on Parallel Plate OAUGDP^{TM} Plasma *47*

Chapter 6. Future Work and Conclusions **52**

6.1 Future Work on Plasma Drift Velocity Measurement by Doppler Effect *52*

6.2 Conclusion *54*

References **56**

Vita **61**

LIST OF FIGURES

FIGURE 2.4.1: ELECTROMAGNETIC WAVE PROPAGATING IN PLASMA. 9

FIGURE 2.4.2: ATTENUATION VERSUS COLLISION FREQUENCY FOR VARIOUS VALUES OF ELECTRON NUMBER DENSITY. 11

FIGURE 2.4.3: PHASE SHIFT VERSUS COLLISION FREQUENCY FOR VARIOUS VALUES OF ELECTRON NUMBER DENSITY. 11

FIGURE 3.1.1: PHOTOGRAPH OF HP 8510C NETWORK ANALYZER SYSTEM AT UT. 12

FIGURE 3.1.2: HP 8510C NETWORK ANALYZER SYSTEM COMPONENTS. 14

FIGURE 3.1.3: INTERCONNECTION OF NETWORK ANALYZER SYSTEM. 14

FIGURE 3.1.4: DIGITAL SIGNAL PROCESSING. 15

FIGURE 3.2.1: FREQUENCY AND TIME DOMAIN MEASUREMENTS. 16

FIGURE 3.2.2: SLIDING LOAD MEASUREMENT IN TIME DOMAIN. 17

FIGURE 3.2.3: MEASUREMENT OF A SLIDING LOAD. 18

FIGURE 3.2.4: TRANSMISSION MEASUREMENT OF A 20 DB ATTENUATOR. 18

FIGURE 3.2.5: TRANSMISSION MEASUREMENT OF AIR LINE. 19

FIGURE 3.2.6: ANTENNA TRANSMISSION MEASUREMENT. 21

FIGURE 3.2.7: ANTENNA TRANSMISSION MEASUREMENT IN TIME DOMAIN. 21

FIGURE 4.1.1: MERCURY-BASED FLUORESCENT LAMP. 24

FIGURE 4.1.2: "MERCURY-FREE" FLUORESCENT LAMP. 25

FIGURE 4.2.1: HORN ANTENNA. 26

FIGURE 4.2.2: HORN RADIATION PATTERNS. 26

FIGURE 4.2.3: BLOCK DIAGRAM OF THE MEASUREMENT SYSTEM. 27

FIGURE 4.2.4: TUBE ARRAY SETUP. 29

FIGURE 4.2.5: METAL LIMITER SETUP. 29

FIGURE 4.3.1: TIME-RESOLVED MEASUREMENT TRIGGERING I. 30

FIGURE 4.3.2: TIME-RESOLVED MEASUREMENT TRIGGERING II. 30

FIGURE 4.3.3: TIME-RESOLVED SAMPLING AT 60 HZ. 31

FIGURE 4.4.1: MEASURED VOLTAGE AND CURRENT DURING ONE AC CYCLE. 33

FIGURE 4.4.2: MEASURED VALUES OF MERCURY-BASED FLUORESCENT LAMP..... 34

FIGURE 4.4.3: MEASURED VALUES OF "MERCURY-FREE" FLUORESCENT LAMP..... 35

FIGURE 4.4.4: CALCULATED PARAMETERS FOR THE MERCURY-BASED FLUORESCENT LAMP..... 36

FIGURE 4.4.5: CALCULATED PARAMETERS FOR THE "MERCURY-FREE" FLUORESCENT LAMP..... 37

FIGURE 5.2.1: FLAT PANEL OAUGDP™ REACTOR. 42

FIGURE 5.2.2: PLASMA PANEL..... 42

FIGURE 5.2.3: MEASUREMENT SYSTEM..... 43

FIGURE 5.2.4: PHOTOGRAPH OF EXPERIMENTAL SETUP..... 44

FIGURE 5.2.5: MICROWAVE SIGNAL PENETRATING FLAT PANEL PLASMA..... 44

FIGURE 5.2.6: ATTENUATION VERSUS RF FREQUENCY. 46

FIGURE 5.2.7: ATTENUATION VERSUS RMS VOLTAGE. 46

FIGURE 5.2.8: ATTENUATION OF PANEL PLASMA AS A FUNCTION OF ELECTRON NUMBER DENSITY. 48

FIGURE 5.2.9: PHASE SHIFT OF PANEL PLASMA AS A FUNCTION OF ELECTRON NUMBER DENSITY. 48

FIGURE 5.3.1: ALIGNMENT OF HORNS FOR PARALLEL-PLATE REACTOR. 50

FIGURE 6.1.1: PARAELECTRIC PANEL. 53

FIGURE 6.1.2: PROPOSED EXPERIMENTAL SETUP FOR DOPPLER EFFECT MEASUREMENT. 53

Chapter 1
Introduction

Plasma is identified as the fourth state of matter. It is an approximately electrically neutral collection of ions and electrons, which may or may not contain a background neutral gas and which is capable of responding to electric and magnetic fields. Plasma engineering is concerned with the application of plasma to devices or processes. Industrial plasma engineering includes the design and application of industrial devices, processes, or products that utilize plasmas. Industrial plasma engineering offers benefits over other industrial processing methods that include the ability to accomplish industrially relevant results more efficiently than competing processes; it usually can accomplish results without producing large volumes of unwanted byproducts or waste materials; and it can usually accomplish results with minimal pollution or production of toxic wastes. Some applications of plasma include plasma enhanced chemistry, surface cleaning, processing of plastics, gas treatment, spraying of materials, chemical analysis, high-efficiency lighting, semiconductor production, TVs and electronics, sterilization of medical devices, and aerodynamic flow control.

Plasma experimental research often requires plasma diagnostics, the means to measure and monitor plasma properties. Plasma diagnostics is concerned with the measurement of such plasma parameters as electron number density, electron kinetic temperature, ion energy distribution, and active species flux. Many plasma diagnostic techniques have been employed in plasma research and its industrial applications, including magnetic probes, Langmuir probes, spectral intensities, far-infrared techniques, optical interferometry, and microwave techniques. With respect to microwave diagnostics, the interpretation of measurements is often difficult and requires not only an understanding of the formal theory of electromagnetic interactions with plasmas, but also the development of intuitive skills in selecting meaningful simplifications. Many plasma-related wave propagation problems are too complicated to permit exact formulation and solution. After World War II, the formulation of a complete theory of wave interaction with plasma and improved

microwave technology stimulated the development of microwave plasma diagnostic methods as standard measuring techniques [1,2].

Microwave plasma diagnostic methods are especially suited to measure the plasma electron number density. Since the electron number density is directly related to the electron plasma frequency for a cold unmagnetized plasma, microwave plasma diagnostic methods have the advantage that almost no model assumptions have to be made with respect to the plasma. Reference [3] compared electron number density measurements using a Langmuir probe and microwave interferometer, and the authors concluded that there is essential agreement between these two methods. Microwave plasma diagnostic research has been focused on the use of microwave interferometers [4-8] to measure the electron number density, with little work focused on measurement of the electron-neutral collision frequency. In this thesis, we apply a sophisticated form of microwave interferometry to measure both electron number density and electron collision frequency simultaneously.

The aim of this thesis is to present a summary of the theory of microwave-plasma interactions and to report data from a microwave diagnostic method that is used to measure the electron number density and electron-neutral collision frequency. This microwave diagnostic method is based on use of a microwave network analyzer. The availability of a modern network analyzer makes it relatively easy to set up a microwave circuit and control the measurements. The diagnostic method measures the attenuation and phase shift of a microwave signal as it passes through plasma. These measured quantities are related to the real and imaginary parts of the plasma index of refraction, described by Appleton's equation [1,2]. Appleton's equation states that the two plasma parameters, electron number density and electron-neutral collision frequency, determine the attenuation and phase shift of a microwave signal as it propagates in a plasma. Reduction of the microwave attenuation and phase shift data using Appleton's equation will yield the electron number density and electron-neutral collision frequency. Since the electron-neutral collision frequency is derived from measured quantities, one need not know the electron energy distribution function, the electron kinetic temperature, or the electron energy-dependent collision cross section.

This study first focuses on the measurement of the properties of a fluorescent lamp plasma, which is a low-pressure normal glow discharge plasma. This thesis also discusses the application of the microwave diagnostic method to the One Atmosphere Uniform Glow Discharge Plasma (OAUGDP^{TM}) [1], an atmospheric pressure glow discharge developed at the UT Plasma Sciences Lab. The contents of this thesis are arranged as follows. Chapter 2 gives a survey of microwave-plasma interactions, and derives the relationship between the plasma electron number density and collision frequency, and the microwave signal characteristics, including the attenuation, phase shift, frequency and signal path. Chapter 3 describes the operation of the network analyzer and several of its features important to the experiment. Chapter 4 presents the experimental setup and discusses the experimental results from two fluorescent lamp plasmas. Measurements on a OAUGDP^{TM} plasma are discussed in Chapter 5. Finally, the conclusions are presented in Chapter 6.

Chapter 2
Theory of Microwave-Plasma Interaction

2.1 Definition of Plasma Parameters

Let us look at the definitions of some plasma parameters before we discuss the microwave - plasma interaction. First is the electron-neutral collision frequency, ν_c. In the partially ionized plasmas prevalent in industrial applications, the particle, momentum, energy, and charge transport properties of the plasma are determined by electron-neutral collisions. The electron collision frequency plays an essential role in determining the power dissipation in the plasma; the energy transfer frequency; and all of the transport coefficients, including the diffusion coefficient, the mobility, the viscosity, the thermal conductivity, and the electrical conductivity. There is a relatively large body of experimental data on the collision cross sections and electron collision frequency in various gases. Reference [1] gives a table of the effective collision frequency, in collisions per second-torr for various gases, taken from Geller and Hosea.

The second significant plasma parameter is the electron plasma frequency ω_{pe}, which plays an important role in determining whether and to what extent an EM wave interacts with plasma. The electron plasma frequency is given by

$$\omega_{pe} = \left(\frac{n_e e^2}{m_e \varepsilon_0}\right)^{1/2} (rad/s), \tag{2.1.1}$$

where e is electronic charge, m_e is the mass of an electron, ε_0 is the permittivity of free space, and n_e is the electron number density in m^{-3}. The electron plasma frequency is the frequency with which electrons oscillate among the heavier, immobile ions when the electron population is disturbed. The electron plasma frequency is critical to the propagation of an EM wave in plasma. When an EM wave propagates towards a plasma, the wave will be mostly transmitted or reflected, depending upon the relationship of the wave frequency ω to the electron plasma

frequency. If the EM frequency is below ω_{pe}, the electrons in the plasma respond to the electric field and extract energy from it. If the EM frequency is above the electron plasma frequency, the electrons have too much inertia to respond o the electric field, and the EM wave is able to propagate through the plasma without significant reflection or attenuation.

2.2 Two EM-Plasma Interaction Modes

If we substitute natural constants into (2.1.1), the electron plasma frequency may be written as $\nu_{pe} = 8.980\sqrt{n_e}$ Hz. If plasma is irradiated with an EM wave of frequency ν_0 , there is a critical electron number density $n_c = 1.2404 \times 10^{-2} \nu_0^2 (electrons/m^3)$, which is derived from the previous expression.

When the frequency of an incident electromagnetic wave ν_0 is below the electron plasma frequency, (i.e. $\nu_{pe} = 8.980\sqrt{n_e}$ Hz, $\nu_0 < \nu_{pe}$,) the inertia of the electrons is low enough for them to respond to the electric field in the incident electromagnetic wave, and the electrons therefore absorb energy from it. This absorbed energy may be converted to heat through collisions, or re-radiated in the form of a reflected electromagnetic wave from the surface of the plasma. Under this condition, the EM-plasma interaction is in the particle interaction regime.

If the frequency of the incident electromagnetic radiation is higher than the electron plasma frequency, (i.e. $\nu_{pe} = 8.980\sqrt{n_e}$ Hz, Hz, $\nu_0 > \nu_{pe}$,) the inertia of an electron is too high to allow it to respond fully to the incident electromagnetic wave. The electromagnetic wave is then free to propagate through the plasma as a quasi-optical dielectric medium, in which the interaction of the electromagnetic radiation with individual electrons is relatively insignificant. In this situation, the microwave - plasma interaction is in the collective interaction regime.

2.3 EM Wave Propagating in Particle Interaction Regime

The electrical conductivity of unmagnetized plasma can be written as

$$\sigma = \frac{n_e e^2}{m_e \nu_c}(S/m), \tag{2.3.1}$$

where e is electronic charge, m_e is the mass of an electron, n_e is the electron number density and ν_c is the electron collision frequency in Hertz.

The propagation constant κ is given by

$$\kappa \equiv \alpha + \mathrm{j}/\delta . \tag{2.3.2}$$

where the real and the imaginary part can be written as

$$\alpha = \sqrt{\frac{\sigma\mu_0\omega}{2}}\left[\frac{\omega\varepsilon_0}{\sigma} + \sqrt{1+\left(\frac{\omega\varepsilon_0}{\sigma}\right)^2}\right]^{1/2} \tag{2.3.3}$$

$$\frac{1}{\delta} = \sqrt{\frac{\sigma\mu_0\omega}{2}}\left[\sqrt{1+\left(\frac{\omega\varepsilon_0}{\sigma}\right)^2} - \frac{\omega\varepsilon_0}{\sigma}\right]^{1/2}. \tag{2.3.4}$$

In the microwave frequency range, the inertia of an electron is too high to allow it to respond fully to the incident electromagnetic wave. Interaction of an electromagnetic wave with plasma in the collective interaction regime is discussed in the next section.

2.4 Attenuation and Phase Shift

A plasma is complicated phenomenon to analyze. Viewed as a medium for electromagnetic waves, a plasma in a magnetic field is refractive, lossy, dispersive, resonant, anisotropic, nonreciprocal, nonlinear, and may be inhomogeneous. We begin the study by proposing as many simplifications as possible. We only consider microwave propagation in an infinite, uniform, unmagnetized, Lorentzian plasma. A

Lorentzian plasma denotes a simplified model in which it is assumed that the electrons interact with each other only through collective space charge forces, and that the heavy positive ions and neutral molecules are at rest. The interaction of electromagnetic radiation with plasma at microwave frequencies usually occurs in the collective regime, where the plasma acts as a dielectric medium, rather than with the electrons individually. In R.B. Gadri's one-dimensional computer model [9], the electron number density of an atmospheric pressure glow discharge plasma is estimated in the order of 10^{11} cm^{-3}. For the microwave frequencies ranging from 12.4 GHz to 18 GHz, the electron number densities are below the critical density of microwaves, which also means the microwave signal interacts with the plasma in the collective interactive regime.

For a homogeneous unmagnetized plasma, the complex index of refraction is given by Appleton's equation [1] [2]

$$\bar{\mu}^2 = (\mu - j\chi)^2 = 1 - \frac{\omega_{pe}^2 / \omega^2}{C_1 \pm C_2^{1/2}}. \tag{2.4.1}$$

where, j is the square root of –1, and ω is the incident microwave frequency in radians. ω_{pe} is the electron plasma frequency given by

$$\omega_{pe} = \left(\frac{n_e e^2}{m_e \varepsilon_0}\right)^{1/2} (rad/s). \tag{2.4.2}$$

where, n_e the electron number density, e is the electronic charge, and m_e is the electron mass.

C_1 and C_2 in (2.4.1) are given by

$$C_1 = 1 - j\frac{\nu_c}{\omega} - \frac{\left(\omega_c^2/\omega^2\right)\sin^2\theta}{2\left[1 - \left(\omega_{pe}^2/\omega^2\right) - j\nu_c/\omega\right]} \tag{2.4.3}$$

$$C_2 = \frac{\left(\omega_c^4/\omega^4\right)\sin^4\theta}{4\left[1 - \left(\omega_{pe}^2/\omega^2\right) - j\nu_c/\omega\right]^2} + \frac{\omega_c^2}{\omega^2}\cos^2\theta \tag{2.4.4}$$

where ω_c is the electron gyrofrequency in the magnetic induction B, given by $\omega_c = \frac{eB}{m_e}$, and ν_c is the electron-neutral collision frequency. When B = 0, $C_2 = 0$. Appleton's equation is simplified and the real index of refraction μ may be written as

$$\mu = \left\{ \frac{1}{2}\left(1 - \frac{\omega_{pe}^{\ 2}}{\omega^2 + \nu_c^{\ 2}}\right) + \frac{1}{2}\left[\left(1 - \frac{\omega_{pe}^{\ 2}}{\omega^2 + \nu_c^{\ 2}}\right)^2 + \frac{\nu_c^{\ 2}}{\omega^2}\left(\frac{\omega_{pe}^{\ 2}}{\omega^2 + \nu_c^{\ 2}}\right)^2\right]^{1/2}\right\}^{1/2}, \tag{2.4.5}$$

and the attenuation index χ is

$$\chi = \left\{ -\frac{1}{2}\left(1 - \frac{\omega_{pe}^{\ 2}}{\omega^2 + \nu_c^{\ 2}}\right) + \frac{1}{2}\left[\left(1 - \frac{\omega_{pe}^{\ 2}}{\omega^2 + \nu_c^{\ 2}}\right)^2 + \frac{\nu_c^{\ 2}}{\omega^2}\left(\frac{\omega_{pe}^{\ 2}}{\omega^2 + \nu_c^{\ 2}}\right)^2\right]^{1/2}\right\}^{1/2}. \tag{2.4.6}$$

Shown in Figure 2.4.1, the propagation equation of an electromagnetic wave in a plasma (lossy medium) is,

$$\begin{aligned} E(z,t) &= \mathrm{Re}\left(E_0 e^{j(\omega t - \kappa z)}\right) \\ &= E_0 e^{-\frac{z}{\delta}} \cos(\omega t - \alpha z) \end{aligned} \tag{2.4.7}$$

where, E_0 is initial electric field intensity, and the angular frequency ω is related to the EM frequency in hertz by $\omega = 2\pi\nu$.

The propagation constant κ in the plasma is given as $\kappa \equiv \alpha + i/\delta$. As discussed previously, the complex refractive index of plasma is defined as $\mu = \mu - j\chi$. The

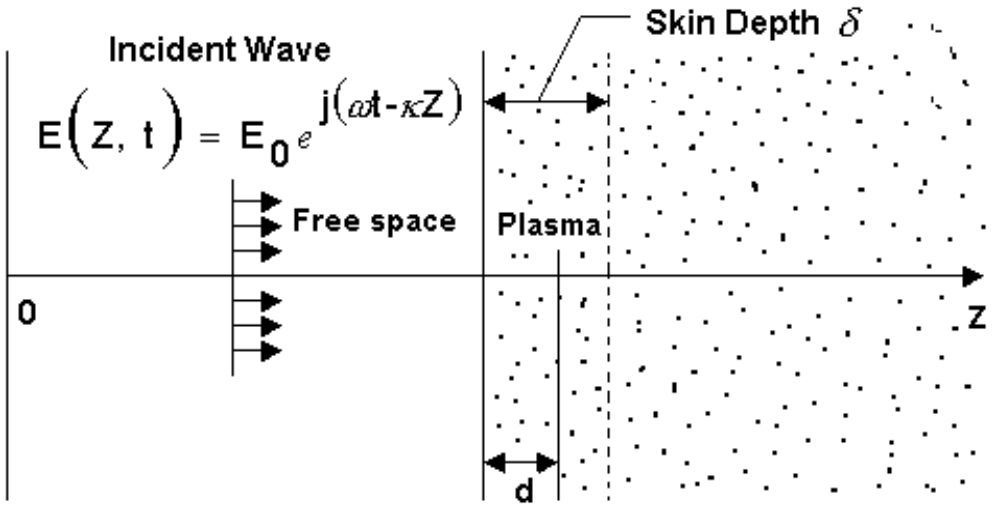

Figure 2.4.1: Electromagnetic wave propagating in plasma.

relationship between the propagation constant and the complex refractive index of plasma is described as follows: α is related to the real refractive index μ by $\alpha = \frac{\omega}{c}\mu$, and $\frac{1}{\delta}$ is related to attenuation index χ by $\frac{1}{\delta} = \frac{\omega}{c}\chi$.

As a plane electromagnetic wave propagates in free space, shown in Figure 2.4.1, The electric field intensity will remain E_0. When a microwave signal propagates in a plasma, the electric field intensity will be attenuated, $E = E_0 e^{-\frac{z}{\delta}}$. Compared to free space, the attenuation of a microwave signal in plasma will be,

$$\alpha(\mathrm{dB}) = 10\log_{10}\left\{\left(\frac{\mathrm{E}}{\mathrm{E}_0}\right)^2\right\} = 10\log_{10}\left(\mathrm{e}^{-\frac{2\mathrm{d}}{\delta}}\right)$$
$$= 10\log_{10}\left(\mathrm{e}^{-\frac{2\mathrm{d}\omega}{\mathrm{c}}\chi}\right) = \mathrm{f}(\mathrm{n_e}, \nu_\mathrm{c}, \omega, \mathrm{d}) \quad . \qquad (2.4.8)$$

When a microwave signal propagates a distance of d in plasma, the phase change is $\phi = \theta_{z2} - \theta_{z1} = \alpha d = \frac{\omega}{c}\mu d$. If in free space, the phase change is $\phi_f = \theta_{z2f} - \theta_{z1f} = \alpha_f d = \frac{2\pi}{\lambda} d$. The term $\frac{2\pi}{\lambda}$ is the wave number in free space. Comparing the phase change when microwave radiation propagates in plasma and in free space, the phase shift is given by

$$\begin{aligned} \Delta\phi(\text{degree}) &= \phi - \phi_f = \left(\frac{\omega}{c}\mu - \frac{2\pi}{\lambda}\right) d \\ &= g(n_e, \nu_c, \omega, d) \end{aligned} \quad . \qquad (2.4.9)$$

Both the attenuation and phase shift become a function of the plasma parameters n_e and ν_c, and the microwave parameters ω and d. For a specific plasma geometry and incident microwave signal, ω and d are constants, and the attenuation and phase shift become functions of n_e and ν_c. If both attenuation and phase shift information are measured, n_e and ν_c can be solved from (2.4.8) and (2.4.9).

Assuming a microwave signal of 15 GHz frequency and a plasma layer 3.8 cm thick, $\omega = 2\pi$ x 15 x 10^9 radians and d = 3.8 cm, Equation (2.4.8) is plotted as a function of electron number density and collision frequency in Figure 2.4.2, and Equation (2.4.9) is plotted as a function of electron number density and collision frequency in Figure 2.4.3. Only n_e = [1x10^{10}, 5x10^{10}, 1x10^{11}, and 5x10^{11}]/cm^3 and 10^9 Hz<ν_c<10^{12} Hz are plotted in the example.

The relationship of the measured microwave values α and $\Delta\phi$ to the plasma parameters n_e and ν_c, illustrated in Figures 2.4.2 and 2.4.3, is the basis of the microwave plasma diagnostic method presented in this thesis. The concept behind the diagnostic method is to make microwave transmission measurements through plasma using a microwave network analyzer system. By measuring the attenuation and phase shift, both the electron number density and the electron collision frequency in the plasma can be derived accurately and in a non-perturbing way. In the next chapter the operation of the microwave network analyzer will be discussed.

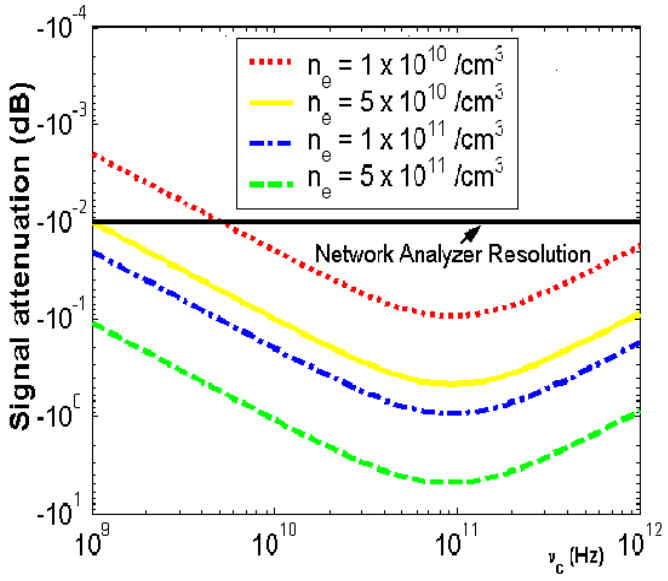

Figure 2.4.2: Attenuation versus collision frequency for various values of electron number density.

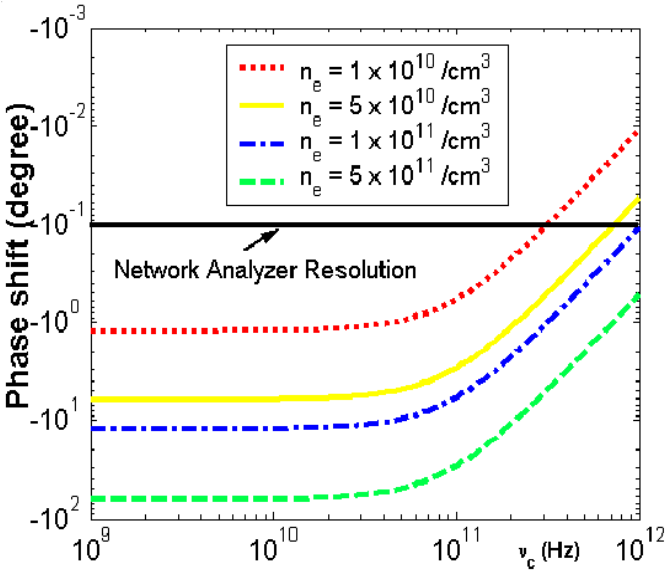

Figure 2.4.3: Phase shift versus collision frequency for various values of electron number density.

Chapter 3
Operation of the Network Analyzer System

3.1 HP 8510C Vector Network Analyzer

The vector network analyzer is a sophisticated measuring instrument designed to make microwave measurements. The basic principles of its operation are relatively simple. For a given two-port device, containing Port 1 and Port 2, the network analyzer can determine the four scattering matrix elements called S-parameters. The input reflection coefficient S_{11}, reverse transmission coefficient S_{12}, forward transmission coefficient S_{21}, and output reflection coefficient S_{22}, all contain amplitude and phase information. The analyzer's internal microprocessor circuitry then processes the S-parameters using smoothing, averaging, and a variety of display formats. The system can simply and efficiently make transmission and reflection measurements. The UT Plasma Sciences Lab has a HP 8510C vector network analyzer system, shown in Figure 3.1.1. The system has an 80-dB dynamic range, 0.01 dB amplitude resolution, 0.1-degree phase resolution, and generates a microwave signal from 0.045 GHz to 18 GHz.

Figure 3.1.1: Photograph of HP 8510C network analyzer system at UT.

The HP 8510C network analyzer is a fully integrated vector network analyzer system. The components of this system include a source, which is a synthesized sweeper to generate the microwave signal; a test set that provides signal separation and the first frequency conversion stage; a receiver (detector) which detects the transmitted or reflected signal; and a display/processor which processes and displays the received signal. These are shown in Figure 3.1.2. The test set transforms the signal, produced by the source, into an incident signal, which is sent to the device-under-test (DUT), and a reference signal, against which the transmitted and reflected signals are later compared. The test set also routes the transmitted and reflected signals from the DUT to the receiver. The receiver converts the microwave signals to a lower intermediate frequency where the signal levels and phase differences can be measured directly. From the calculated value, the reflection and transmission characteristics of the device can be derived. Using its internal microprocessor, the system performs signal averaging to enhance accuracy and displays the result in a variety of formats. Measurement results can be sent to additional system accessories, including a printer, a plotter, and a disc drive. These accessory instruments may be controlled manually with network analyzer front panel keys.

The UT Wireless Communication Lab possesses an Agilent 83622B synthesized sweeper, which is compatible with the 8510C network analyzer system and replaces the original HP8350B microwave signal generator. The 83622B sweeper has a 1 Hz frequency resolution and external triggering features, which the 8350B lacks. Especially important for our application, the external triggering feature synchronizes the data acquisition cycle with an external trigger signal provided at the rear-panel connection of the sweeper, and allows time-resolved measurement of attenuation and phase shift, as will be discussed later.

Figure 3.1.3 illustrates the interconnection of the HP8510C system. The microwave-synthesized sweeper is capable of sweeping over a desired frequency range, which may be from 45 MHz to 100 GHz depending on the source model. Our system can sweep from 0.045 GHz to 18 GHz. Figure 3.1.4 shows the digital processing logic of the internal microprocessor.

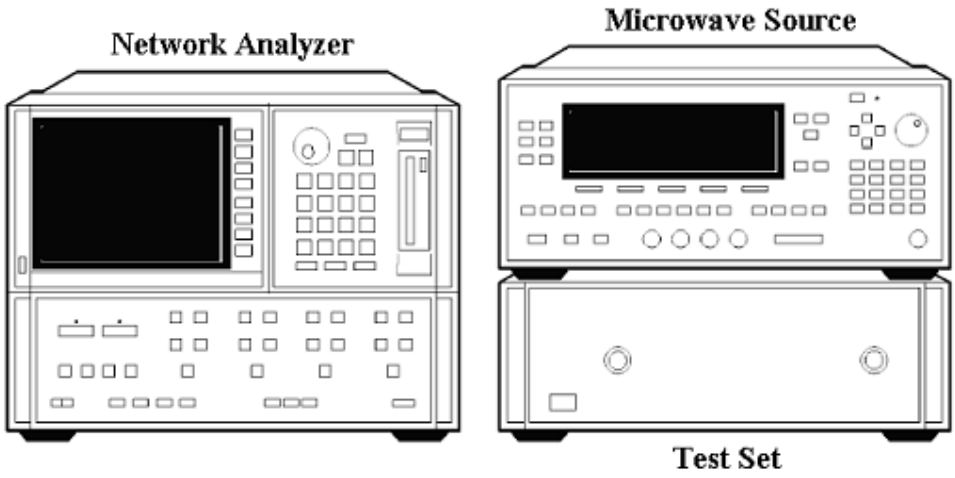

Figure 3.1.2: HP 8510C network analyzer system components.

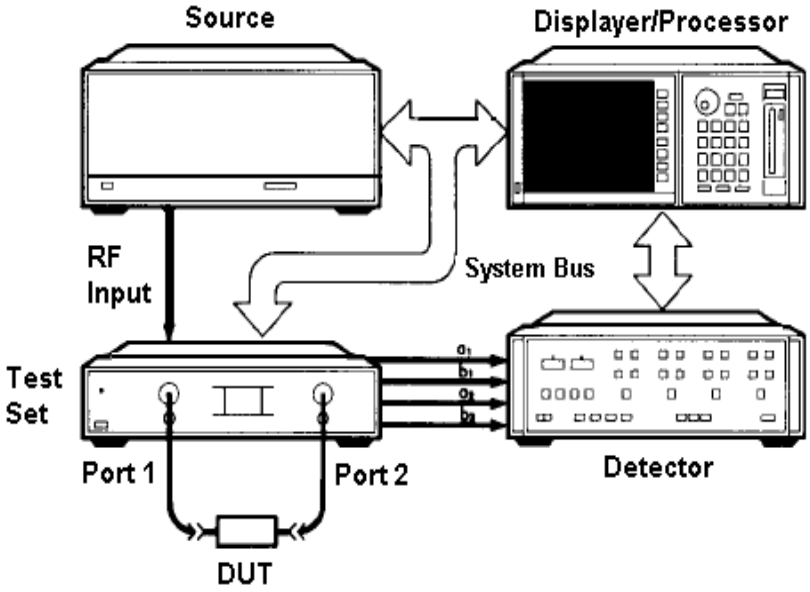

Figure 3.1.3: Interconnection of network analyzer system.

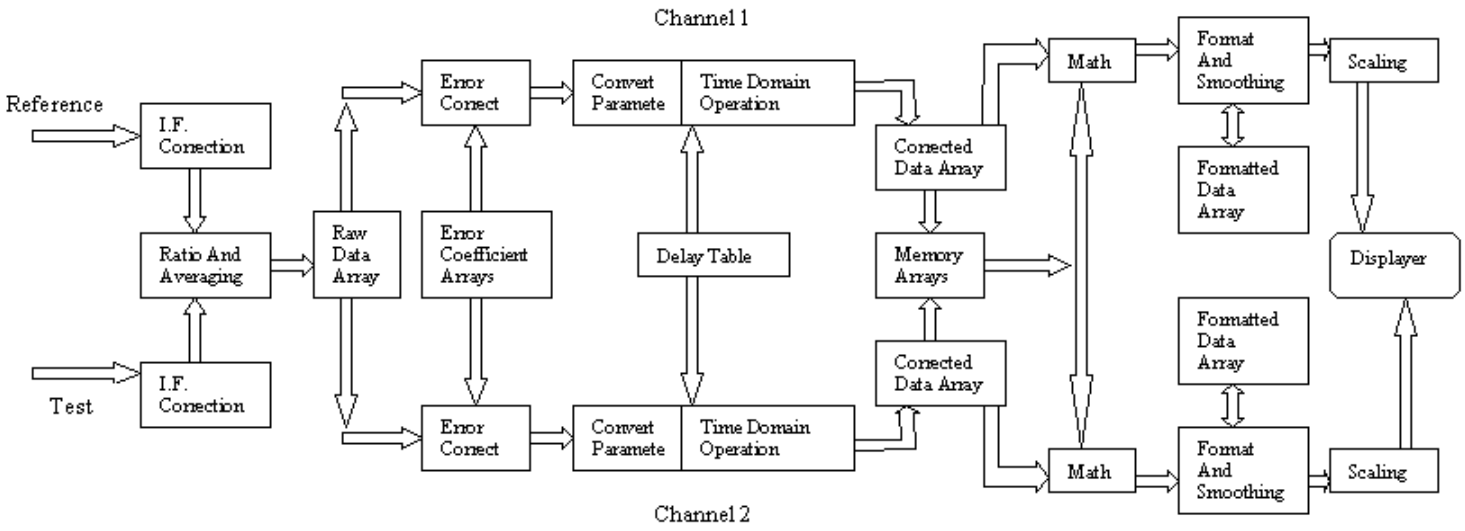

Figure 3.1.4: Digital signal processing.

3.2 Time Domain Measurement

In the previous section, we discussed the operating principles of the network analyzer. The network analyzer also provides many system features that make possible simple and accurate microwave reflection and transmission measurements. One of the features we use in the experimental work is time domain measurement. This section discusses the principles of time domain measurement and how to incorporate this function into our diagnostic method.

In the network analyzer, all measurements are made in the frequency domain. However the frequency domain response can be mathematically transformed into a time domain response by the internal microprocessor. The relationship between the frequency domain response H(f) and the time domain response h(t) in a network is described by a Fourier transform. It is therefore possible to measure the response of a device in the frequency domain, and then mathematically calculate the inverse Fourier transform of the data to give the time domain response. The microprocessor of the HP8510C network analyzer calculates the time domain response using Chirp-Z Fast Fourier Transform computation techniques. The resulting measurement is the fully error-corrected time domain response, reflection or transmission, of the device. The result can be displayed in real-time. Figure 3.2.1 shows the frequency and time domain reflection responses of the same device.

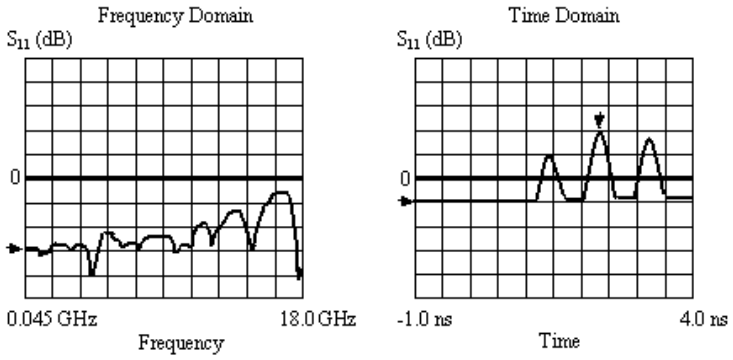

Figure 3.2.1: Frequency and time domain measurements.

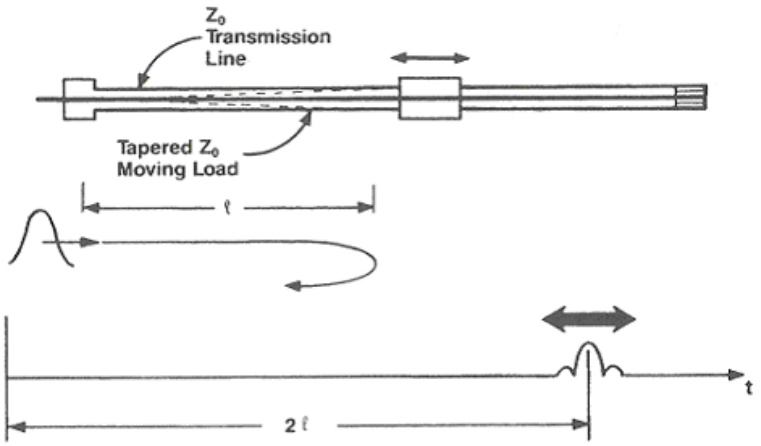

Figure 3.2.2: Sliding load measurement in time domain.

In the time domain reflection measurement, the horizontal axis represents the time required for an impulse, launched at the test port, to reach the discontinuity and return. Thus, this is a two-way travel time to the discontinuity, which in Figure 3.2.2 is the load element of the sliding load. In Figure 3.2.3, the marker reads out both the time and the electrical length to the discontinuity. The electrical length is obtained by multiplying the time by the velocity of light in free space (2.99×10^8 m/sec). To get the physical length, one multiplies the displayed electrical length by the relative velocity of light in the transmission medium. The quantity displayed on the vertical axis gives the magnitude of the reflection. It is an average reflection coefficient of the discontinuity over the frequency range of the measurement.

The time domain mode is also useful in making transmission measurements. It provides the means to analyze the length and attenuation of multiple signal propagation paths of the device, which is extremely useful in our experiment. Figure 3.2.4 shows the frequency and time domain responses of a 20 dB attenuator.

The horizontal axis is displayed in units of time, which indicates the propagation delay or electrical length of the measured device connected between the two test ports of the network analyzer. The value displayed is the actual electrical length, read out in both time and distance. One must multiply the distance by the relative propagation

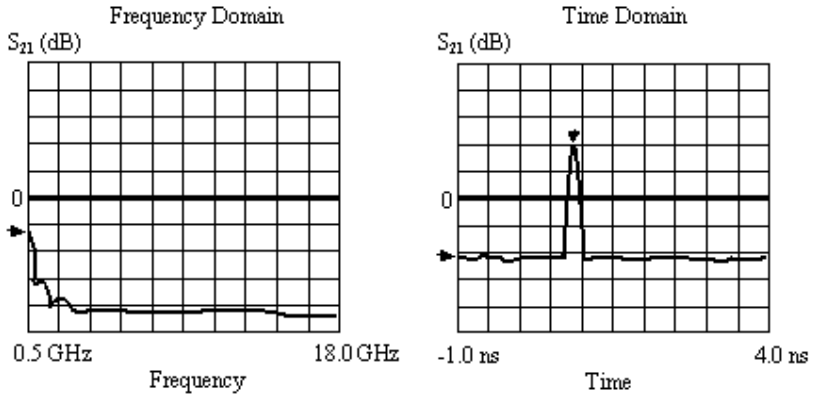

Figure 3.2.3: Measurement of a sliding load.

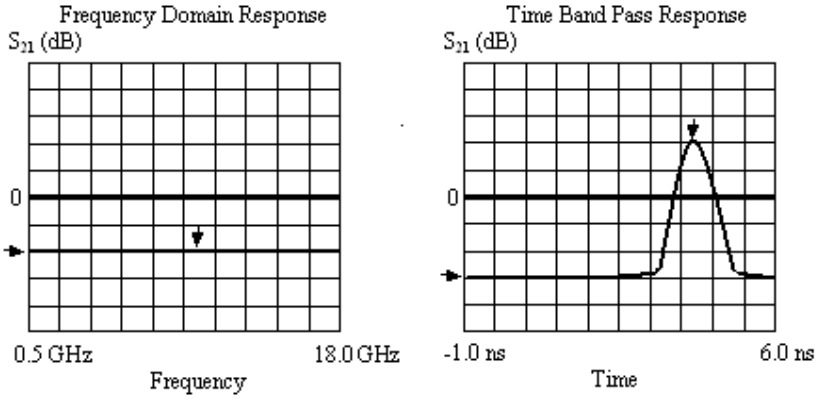

Figure 3.2.4: Transmission measurement of a 20 dB attenuator.

velocity of the transmission medium to get the physical length. The vertical axis displays the transmission coefficient, the transmission loss or gain. This can be thought of as an average transmission coefficient of the signal path over the frequency range of the measurement. For the measurement of a 20 dB attenuator the peak mark has a magnitude of 0.10 transmission coefficient units, which is a 20 dB insertion loss.

Multiple-path signals are a major form of interference in microwave propagation measurements. The network analyzer's time-domain mode provides a method to distinguish the multiple-path signal from the main path signal. For a device under test, if there are multiple transmission paths through the device, the magnitude response of each path will be measured and displayed. Figure 3.2.5 shows the transmission response of a 30 cm air line. The larger impulse is the direct (main) path response through the air line. The second, lower level impulse is the triple-travel path through the air line, which is caused by the impulse reflecting back and forth between the mismatches at the ends of the air line.

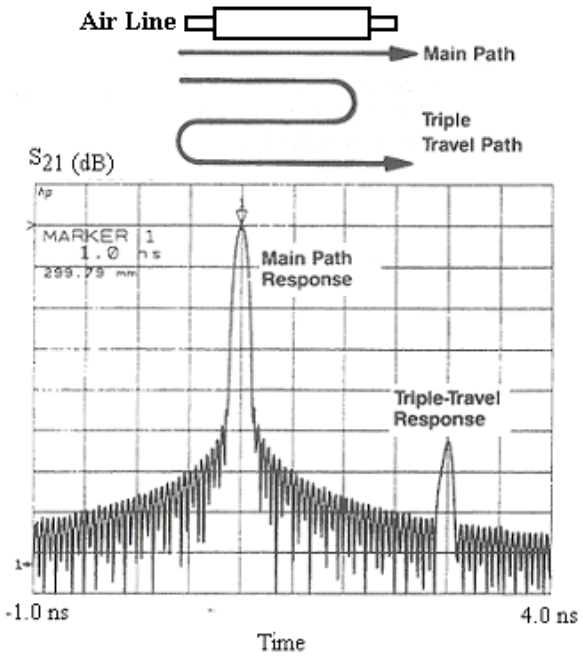

Figure 3.2.5: Transmission measurement of air line.

The plasma diagnostic method discussed in this thesis is based on a microwave free space transmission measurement using horn antennas. Let us consider a horn antenna measurement setup shown in Figure 3.2.6. In this type of measurement there is often an unwanted bounce path reflection that interferes with the desired main path measurement. The time domain response shown in Figure 3.2.7 clearly identifies the main path response between the two antennas, as well as the bounce path response reflected from the ground plane. This is a very valuable measurement tool. For reflection measurements, the horizontal axis shows the 2-way travel time of the impulse at the point where the impulse is reflected. By placing a marker on the peak of the response, one can measure the 2-way travel time and travel distance directly.

3.3 External Triggering

Triggering plays an important role in our experiment setup. This section gives an overview of the network analyzer's external triggering feature. The vector network analyzer supports three different trigger sources: 1.) an internal trigger, in which the network analyzer supplies continuous trigger signals; 2.) a manual trigger, in which the user supplies a trigger signal by pushing a front panel button; 3.) an external trigger, in which the trigger signal is supplied by external hardware. Typically in an antenna measurement setup, the network analyzer is externally triggered. This is required to synchronize the network analyzer's data collecting with other hardware such as signal sources and antenna positioners. When applying an external trigger, a pulsed signal is fed to the network analyzer's rear-panel Trigger input, and the data acquisition cycle is triggered on the falling edge of the external pulsed signal.

The network analyzer must be set to "external trigger" in the step-sweep mode in order to apply an external edge trigger. It goes through the following process upon receiving a trigger signal. 1. External Trigger received. 2. Ready for trigger goes high (inactive, this occurs within a couple of μs after the trigger signal is received). 3. System setup (sweeping frequency, gain ranging, anti-alias filter settling, etc.). The time required is typically 70 μs in step-sweep mode. 4. Data acquisition, the time for which is roughly 1 / (IF Bandwidth). The IF bandwidth is usually 10 KHz. 5. Step to

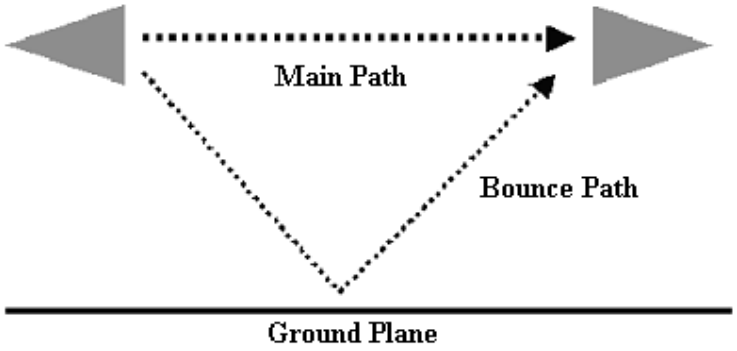

Figure 3.2.6: Antenna transmission measurement.

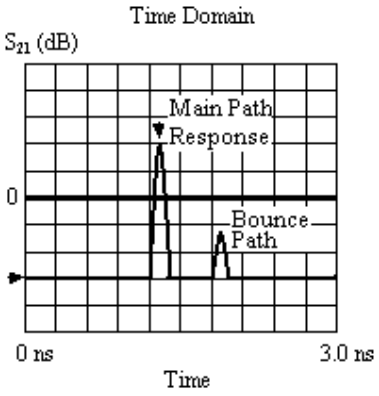

Figure 3.2.7: Antenna transmission measurement in time domain.

next frequency. The above time values are quoted from the manual of the Agilent PNA series network analyzer, a model which has a much higher measurement speed

than the HP 8510C vector network analyzer. For the 8510C system, the exact time delay after a pulsed signal is not known, and the only documentation is that the trigger pulse must remain "on" for at least 1 millisecond. This means, at best, that the maximum measurement speed cannot exceed 1 KHz. The practical measurement speed also depends on the configuration of the network analyzer and the actual performance of the system. Our tests show that the HP 8510C system in the Plasma Sciences Lab has a 100-Hz maximum measurement speed when applying an external trigger. However, when an internal trigger source is used, the maximum measurement speed is 4 KHz.

The triggering capabilities of the network analyzer make it a powerful tool in a variety of measurement applications. The edge and point triggering features allow precision synchronization with other components of an antenna measurement system; and these features are easily applied to other measurement applications as well. The next chapter explains how these features can be employed in our time-resolved measurement setup.

Chapter 4
Measurement of a Fluorescent Lamp Plasma

4.1 Fluorescent Lamp

A fluorescent lamp is a specialized gas discharge tube. A pair of electrodes, one at each end, are sealed along with a drop of mercury and an inert gas (usually argon) at a pressure of 1-3 Torr inside a glass tube. The inside of the tube is coated with a phosphor, which produces visible light when excited by ultra-violet (UV) radiation. When the lamp is off, the mercury/gas mixture is non-conductive. When power is first applied, a high voltage (several hundred volts) is needed to initiate the discharge. However, once this takes place, a much lower voltage, which is usually under 100 V for tubes under 30 watts, 100 to 175 volts for 30 watts or more, is needed to maintain it. Fluorescent lamps are about 2 to 4 times as energy efficient as incandescent lamps at producing photons at wavelengths visible to humans. Thus, they run cooler for the same effective light output. The bulbs themselves also last a lot longer - 10,000 to 20,000 hours vs. 1000 hours for a typical incandescent bulb.

The inert gas and mercury vapor produce plasma inside the lamp tube when the lamp is energized. The power line makes one electrode electrically positive, the other negative causing ions to be accelerated towards the negative end, and electrons to the positive end. The accelerated electrons gain energy, collide with atoms, produce additional electrons by ionization and thus maintain the plasma, even if some other particles re-combine. Inelastic electron collisions raise electrons in mercury atoms to higher energy levels, and these excited atoms then emit ultraviolet photons when they drop into lower energy levels.

We used standard commercial fluorescent lamps in our experiment. We measured both the previously standard mercury-based and the recent “mercury-free” fluorescent lamp plasmas. The mercury-based lamp is a 33-Watt General Electric Bright Stick (see Figure 4.1.1). The tube length is 63.5 cm and the tube diameter is 3.8 cm. The tube is filled with an Ar-Hg mixture. Argon is at the rated pressure of 3 Torr; Hg vapor is at 10^{-4} to $5\text{x}10^{-3}$ Torr depending on the tube wall temperature. The

Figure 4.1.1: Mercury-based fluorescent lamp.

"mercury-free" lamp is a 20-Watt Philips F20T12 Alto, the dimensions of which are same as GE Bright Stick. The fluorescent lamps are connected to a 60 Hz, 120 Vrms AC power line. The lamp tube is placed between two microwave horns facing each other.

Currently, all fluorescent lamps contain mercury for effective operation. Although mercury is essential for fluorescent lamp operation, it is a volatile metal that can pass into the atmosphere during waste combustion and leach into the ground from municipal landfills, contaminating water, fish and food supplies. The technology employed by industrial manufacturers, such Philips and General Electric, places the mercury in precise amounts within a small capsule, and uses it in combination with a proprietary chemical buffering system and special phosphors within the tube. The reduction of mercury in these lamps is approaching 70% compared to conventional manufacturing processes. Shown in Figure 4.1.2, the "mercury-free" lamp has distinctive green end caps.

Figure 4.1.2: “Mercury-free” fluorescent lamp.

4.2 Measurement System

Horn antennas are used for microwave transmission and reception. The transmitting and receiving horns are standard commercial Ku-band (12.4 – 18 GHz) rectangular horns with 20-dB gain, manufactured by the Advanced Technical Material Inc. Shown in Figure 4.2.1, the physical size is A = 7.32 cm, B = 5.36 cm, C = 14.6 cm. The radiation patterns are shown in Figure 4.2.2 and the full angle 3dB beam width is E-plane 18.8^0 in the E-plane and 18.9^0 in the H-plane. The horns are separated by a distance of 50 cm, and therefore operate in the far field mode for the 15 GHz transmitting signal. The horns are positioned in such a way that the signal propagation direction is perpendicular to the axis of the fluorescent tube and intercepts only the middle of the tube.

This measurement system is based on our HP 8510C vector network analyzer. This system consists of five components: the network analyzer, horn antennas, a pulse generator, a current monitor for the fluorescent lamp, and support structure. A frame was fabricated to support the horns and the fluorescent light tube and keep them well

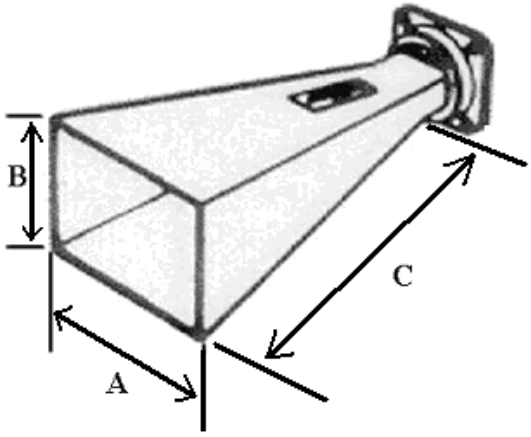

Figure 4.2.1: Horn antenna.

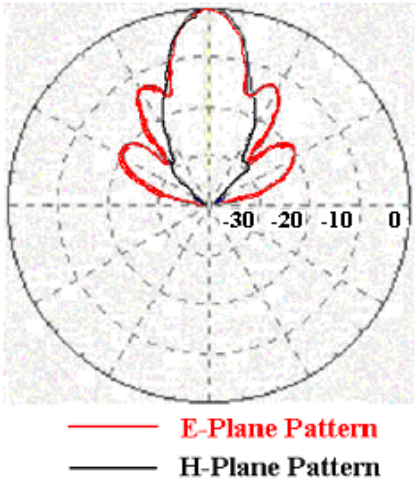

Figure 4.2.2: Horn radiation patterns.

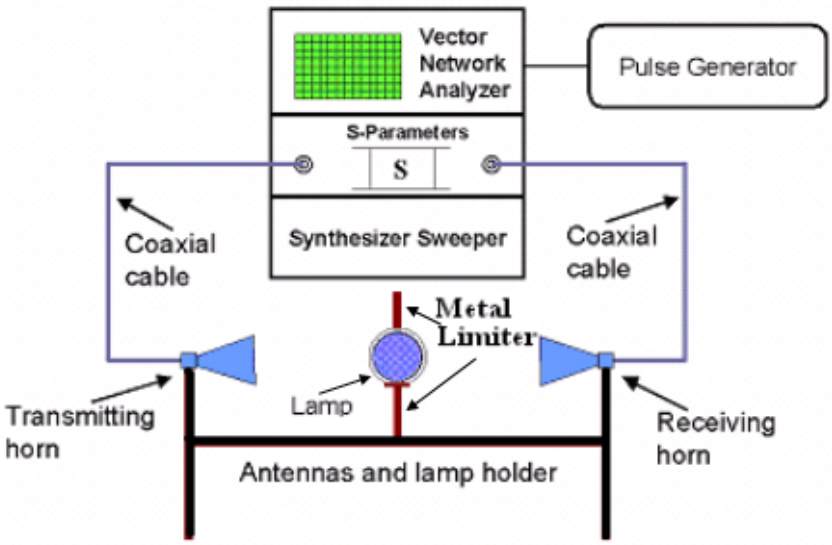

Figure 4.2.3: Block diagram of the measurement system.

aligned. We achieved satisfactory alignment by adjusting the position of the horns and maximizing the received signal. The configuration of the measurement system is illustrated schematically in Figure 4.2.3.

We used the external triggering feature of the network analyzer to make time-resolved measurements. Each falling edge of the pulse signal triggers a data acquisition cycle of the network analyzer. When making measurements on the fluorescent lamp plasma, a Hewlett Packard 214A pulse generator produces a 60-Hz power-line-synchronized pulsed signal to trigger the network analyzer measurement. A time-resolved measurement can be made by adjusting the position and falling edge of the pulse through the whole plasma cycle. We used a 2100 Wide Band current monitor, produced by Pearson Electronics Inc to monitor the plasma current. The details of time-resolved measurements will be discussed in the next section.

As shown in Figure 4.2.3, the fluorescent lamp tube is place between two horn antennas. The diameter of the tube is 3.8 cm, and the rectangular opening of the horn (Figure 4.2.1) is 7.32 cm x 5.36 cm. Therefore the microwave beam is wider than the

tube and significant signal would go around instead of through the tube. Two experimental setups were considered to block the signal around the tube. One is shown in Figure 4.2.4. A tube array is constructed, so that all microwave signals will go through fluorescent lamp tubes. The other is illustrated in Figure 4.2.5, in which a metal limiter is used to block the signal that goes around the single tube. The metal limiter is used in our experiment.

4.3 Time-Resolved Measurement Configuration

The details of the time-resolved measurement configuration will be discussed in this section. The external trigger feature discussed in Chapter 3 is the most important feature for time-resolved measurements. The external trigger feature synchronizes the data acquisition cycle with an external triggering signal provided at the rear-panel connection of the sweeper. This allows the system measurement sequence to synchronize with an externally provided pulse sequence. Measurement by the network analyzer is triggered by the falling edge of the triggering pulse. By adjusting the position of the pulse within a period of the 60 Hz power line AC voltage, the network analyzer can make measurements at any point during an AC plasma cycle, thus allowing time-resolved measurement.

There are two ways to make time-resolved measurements. One is shown in Figure 4.3.1, and may be used when the measurement speed is high compared to the RF or AC plasma driving frequency. In this case, the network analyzer can measure several points during one AC plasma cycle. If the measured points lie across more than one AC cycle, the sampled data must be periodic with the plasma driving signal.

In the second situation, in which the plasma driving frequency is too high for the network analyzer to make more than one measurement in a plasma cycle, only one datum can be acquired during one or several plasma cycles (see Figure 4.3.2). However, the time-resolved characteristics of the plasma still can be measured. As shown in Figure 4.3.2, the measurement is controlled by an external triggering pulse. The plasma driving signal and the external triggering pulse are synchronized with each other. The measurement is triggered by the falling edge of the pulse. It is still

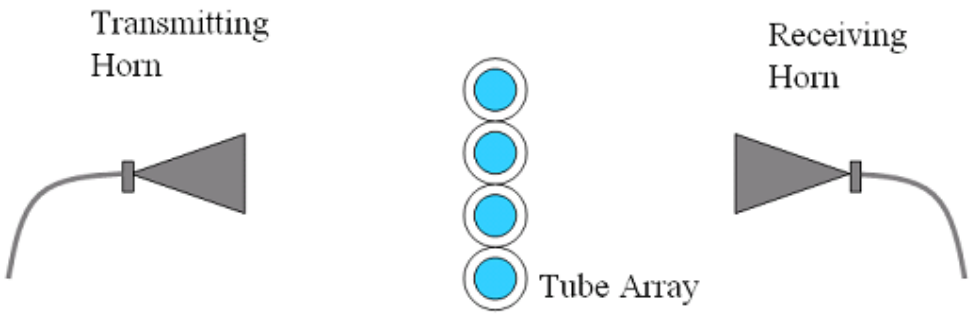

Figure 4.2.4: Tube array setup.

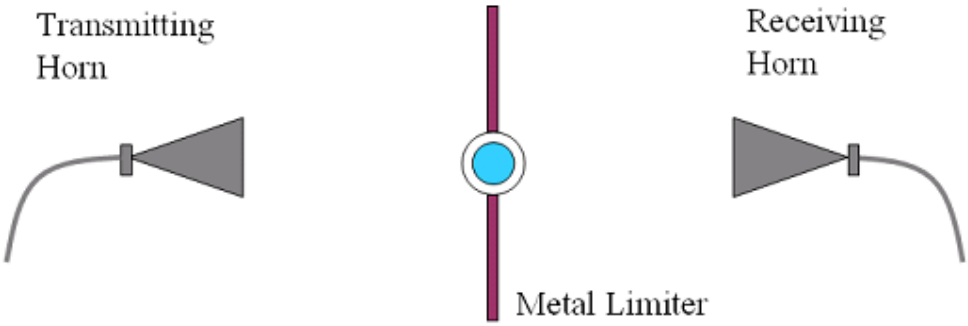

Figure 4.2.5: Metal limiter setup.

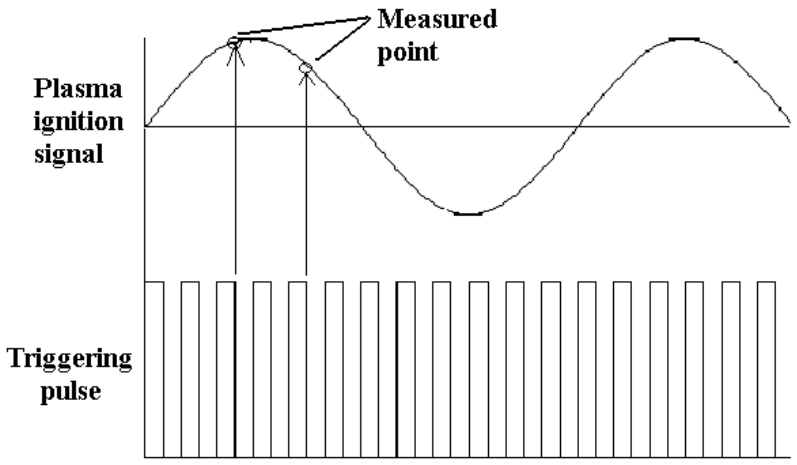

Figure 4.3.1: Time-resolved measurement triggering I.

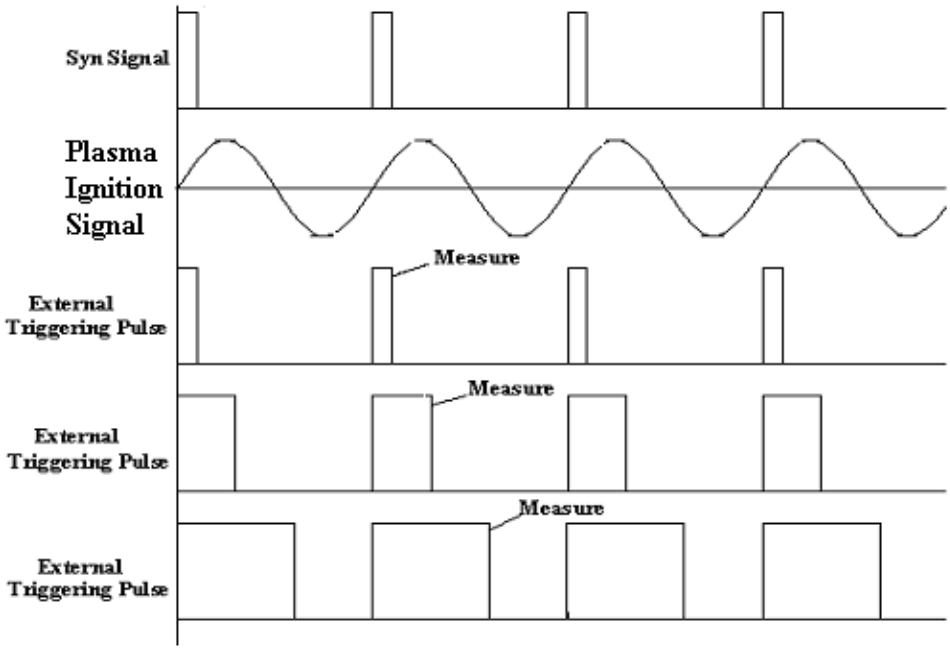

Figure 4.3.2: Time-resolved measurement triggering II.

possible to program to sample the data at any position during one cycle of the plasma driving signal by adjusting the width of the external triggering pulse or the position of each pulse.

When applying external triggering, the maximum sampling speed for the HP 8510C network analyzer system is only 100 Hz. The fluorescent lamp was connected to a 60-Hz, 120-Vrms AC power line. Therefore, the method illustrated in Figure 4.3.2 was used to make time-resolved measurements of the fluorescent lamp plasma. A 60 Hz pulsed signal, which is synchronized with the plasma driving signal, is fed to the network analyzer system to trigger measurements. Since the position of the falling edge of each pulse can be adjusted, the periodic variation of the fluorescent lamp plasma characteristics can be measured. Figure 4.3.3 shows the waveform of the triggering signal and the power line voltage monitored by an oscilloscope.

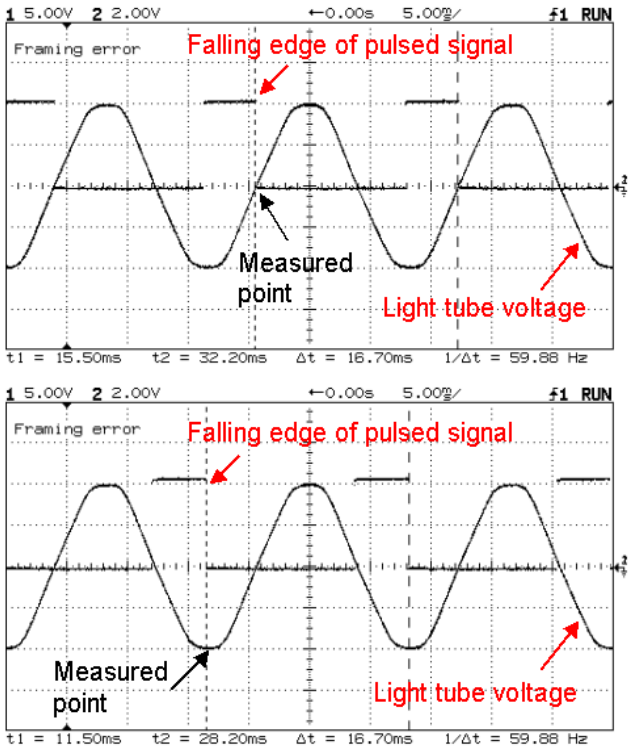

Figure 4.3.3: Time-resolved sampling at 60 Hz.

4.4 Measured and Calculated Results

The fluorescent lamp was connected to a standard 60 Hz power line. A current monitor is used to measure the current through the lamp tube. An oscilloscope is used to measure and display the voltage and current. Shown in Figure 4.4.1, the peak current is 520 mA for the "mercury-free" lamp and 340 mA for the conventional mercury-based lamp. The measurements show that the average current through "mercury-free" lamp tube is higher than the average current through the mercury-based lamp tube.

For time-resolved measurements, we measure the attenuation and phase shift of the transmitted microwave signal during one plasma cycle, and then derive the electron number density and collision frequency of the plasma. The measured data are plotted in Figure 4.4.2 and Figure 4.4.3. Figure 4.4.2 shows data from mercury-based fluorescent lamp and Figure 4.4.3 from "mercury-free" fluorescent lamp.

In both figures, part (a) plots the plasma current in one cycle with 43 sampling points. Parts (b) and (c) show the measured value of microwave attenuation and phase shift at these sampling points. The plasma number density in the fluorescent lamp tube is directly related to the plasma current. Higher current will result in a higher electron number density in the tube. From Figure 4.4.2 and Figure 4.4.3, the peak value of the current is in the vicinity of the peak value of the measured attenuation and phase shift.

The electron number density and collision frequency, calculated from Appleton's equation and equations (2.4.8) and (2.4.9), are shown in Figure 4.4.4 and Figure 4.4.5. The electron number densities vary during the plasma cycle. The waveform of the collision frequency is more complicated than that of the electron number density. Collision frequencies in noble gases were investigated in [10] and [11]. The collisional process in fluorescent lamps was also studied in [12].

According to the calculation, the electron number density of the mercury-based fluorescent lamp plasma ranges from $3.5 \times 10^{10}/cm^3$ to $2.6 \times 10^{11}/cm^3$, and the

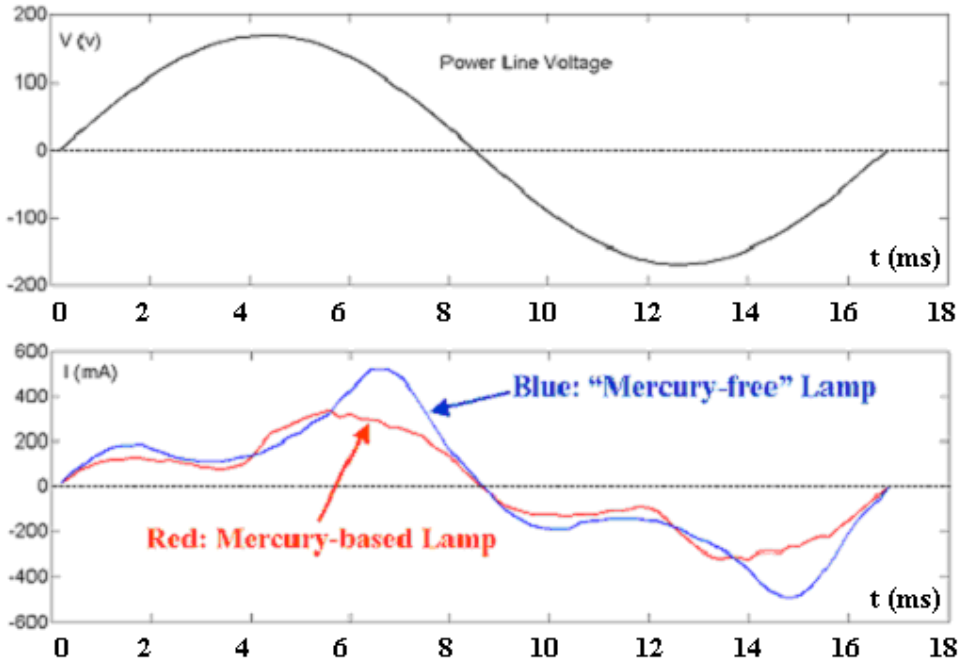

Figure 4.4.1: Measured voltage and current during one AC cycle.

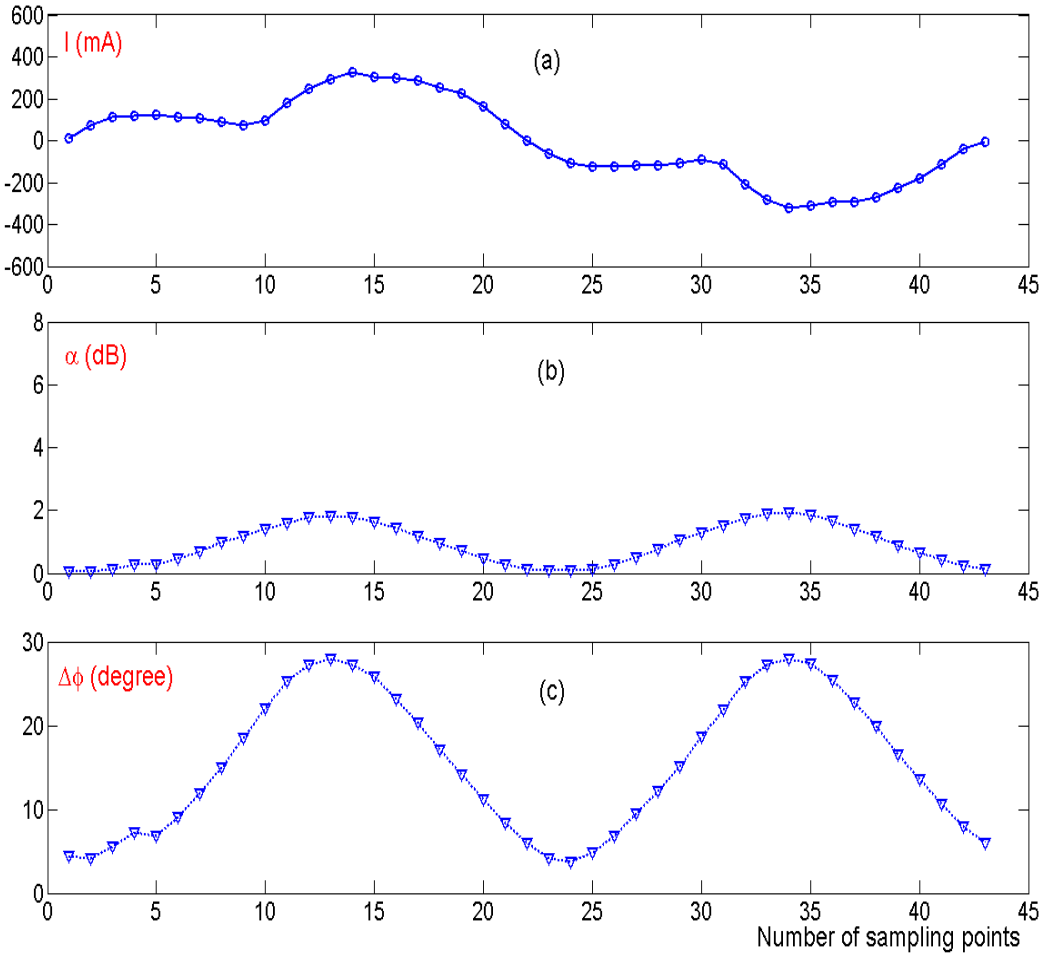

Figure 4.4.2: Measured values of mercury-based fluorescent lamp.

(a) Lamp current at sampling points in one cycle (b) Measured attenuation (c) Measured phase shift.

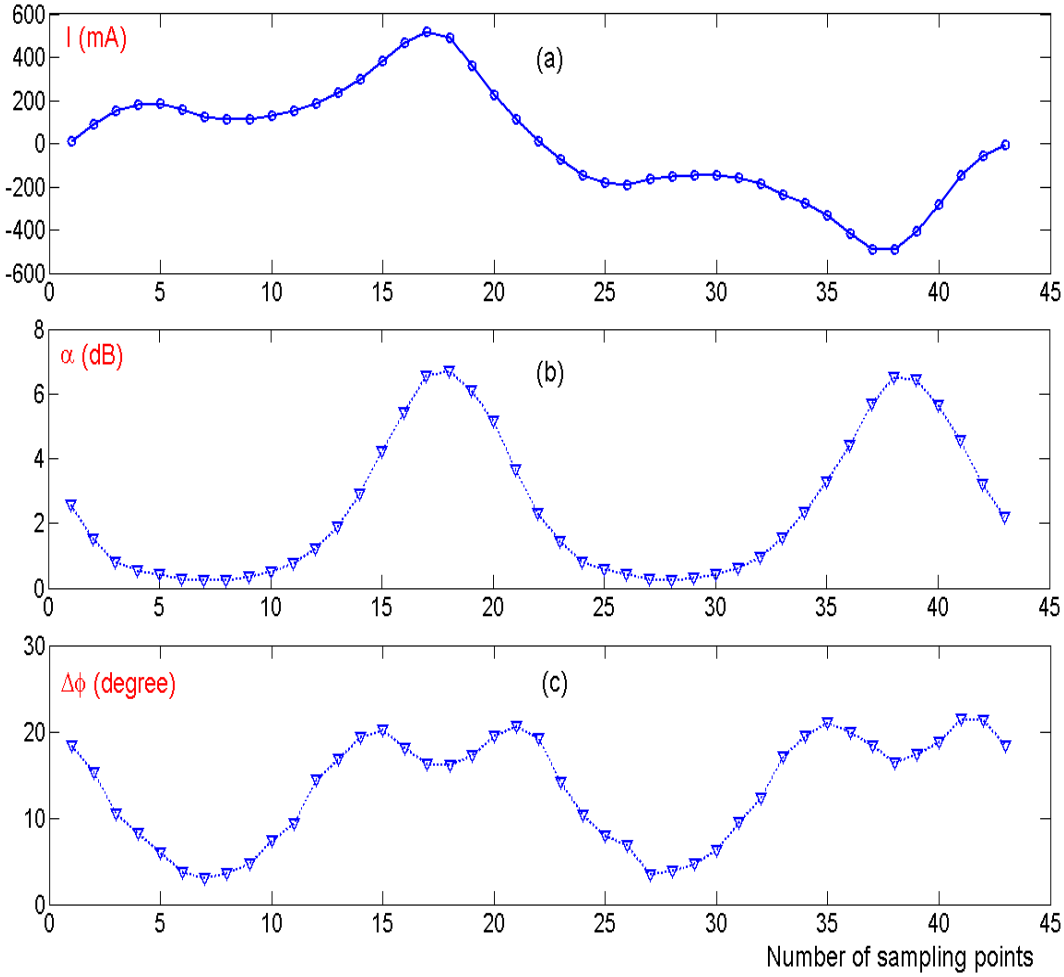

Figure 4.4.3: Measured values of "mercury-free" fluorescent lamp.

(a) Lamp current at sampling points in one cycle (b) Measured attenuation (c) Measured phase shift.

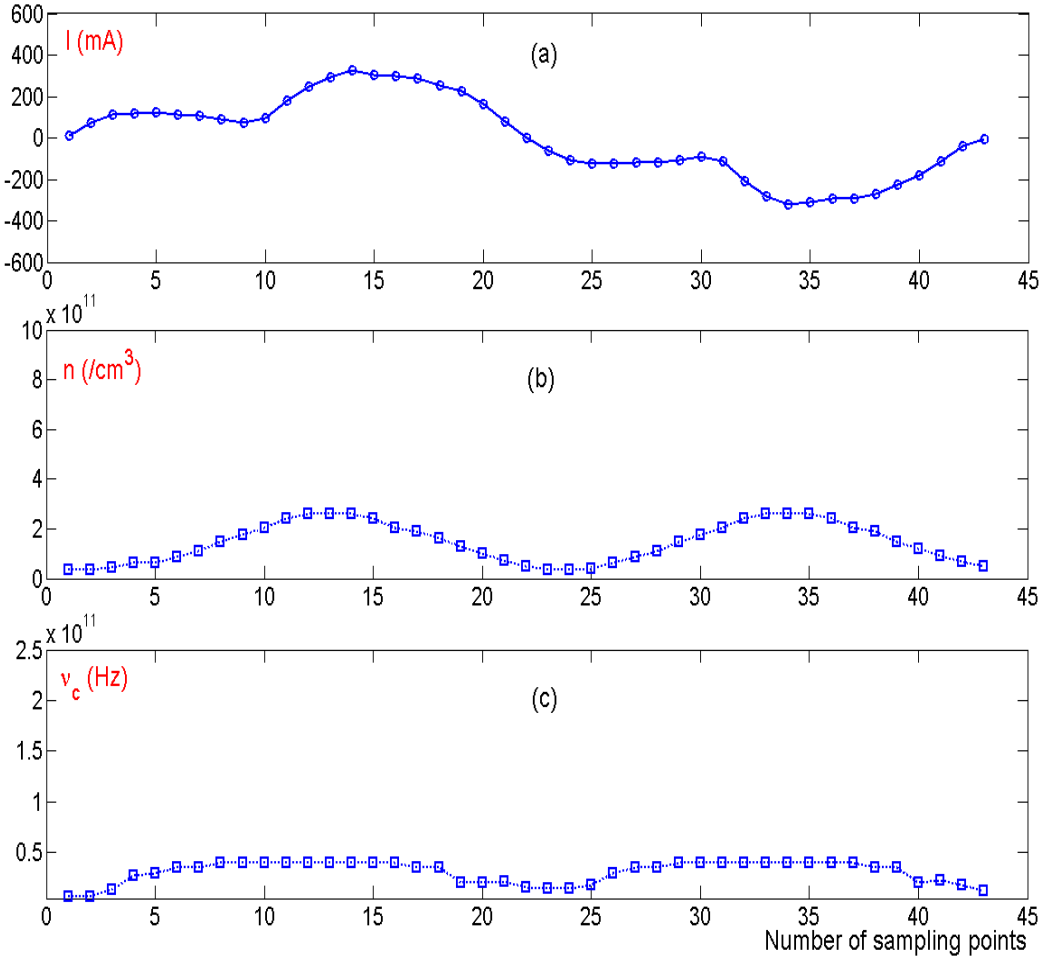

Figure 4.4.4: Calculated parameters for the mercury-based fluorescent lamp.

(a) Lamp current at sampling points in one cycle (b) Calculated electron number density (c) Calculated electron collision frequency.

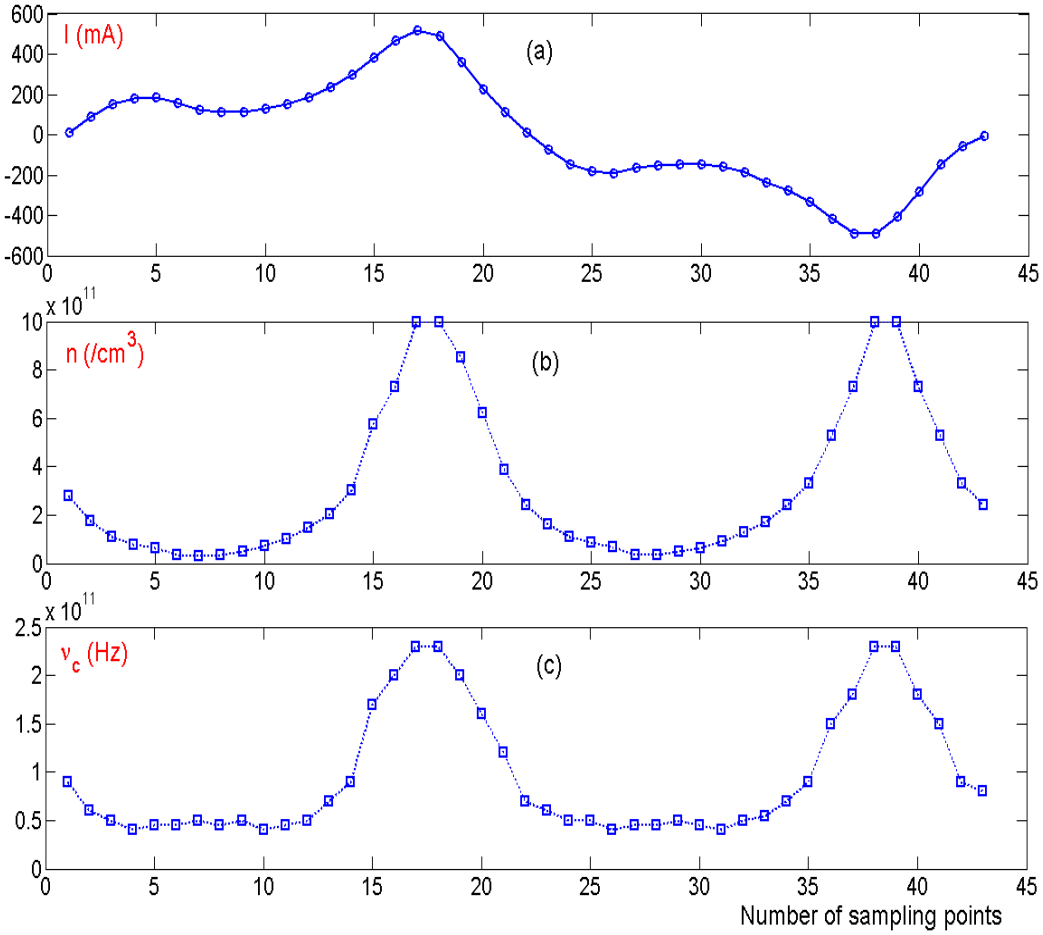

Figure 4.4.5: Calculated parameters for the "mercury-free" fluorescent lamp.

(a) Lamp current at sampling points in one cycle (b) Calculated electron number density (c) Calculated electron collision frequency.

collision frequency is from 7 x 10^9 Hz to 4 x 10^{10} Hz. The electron number density of the mercury-free fluorescent lamp plasma ranges from 3.0 x 10^{10}/cm^3 to 1 x 10^{12}/cm^3, and the collision frequency is from 4 x 10^{10} Hz to 2.3 x 10^{11} Hz. The author in [13] applied the double Langmuir probe diagnostic method to microwave resonant cavity discharges and the analysis predicted time-averaged electron number densities from 10^{11}/cm^3 to 3 x 10^{12}/cm^3, and collision frequencies from 10^9 Hz to 10^{11} Hz. The experiments in [14] yielded an electron number density of 7 X 10^{10}/cm^3 for argon gas at a pressure of 100 mTorr. In [15], Thomson scattering was used to determine the time-averaged electron number density in a low-pressure argon-mercury positive column, which ranges from 5 x 10^{11}/cm^3 to 1.5 x 10^{12}/cm^3 on the axis of the tube.

Chapter 5
Measurements of a OAUGDP™ Plasma

In Chapter 4, we presented measured results from a 60 Hz low-pressure fluorescent lamp plasma. Here, we extend our diagnostic method to time-averaged measurements of the OAUGDP™ plasma, operating in air at one atmosphere.

5.1 Atmospheric Pressure Plasma Diagnostics

Research on partially ionized atmospheric pressure glow discharge plasmas is motivated by applications such as surface treatment of fabrics, plasma sterilization, and subsonic plasma aerodynamics. The main advantage of atmospheric pressure plasmas for many applications is the much greater flexibility afforded by the absence of a vacuum vessel. In principle, this allows large-scale, continuous processing instead of the small-scale batch processing associated with low-pressure plasmas. The absence of a vacuum system will also reduce the processing cost significantly. The development of atmospheric pressure plasma sources to replace plasma processing in a vacuum environment is a current trend in industrial plasma engineering. Since the industrial application of atmospheric pressure plasma has just begun, the plasma diagnostics required for process control have not yet been fully explored. Some research work has been reported in [16, 17]. In [16], an optical emission spectroscopic method was used to determine the distribution of the plasma density by means of Abel inversion analysis. In [17], an infrared heterodyne interferometer has been used to measure the spatial distribution of the electron number density in atmospheric pressure discharges in air. Other diagnostic techniques such as Thomson scattering and Langmuir probe measurements are well established for low-pressure plasmas, but their potential for application to atmospheric pressure glow discharge plasmas has not been explored. A glow discharge at atmospheric pressure has an electron mean free path less than one micron. This is well below the Debye shielding distance, seriously compromising the use of conventional Langmuir probe theory to obtain the electron number density or kinetic temperature in this regime.

As a well-established non-perturbing diagnostic method, microwave interferometry is widely used to measure the electron number density of DC and RF glow discharge plasmas. Since the electron number density is directly related to the

plasma frequency (in the approximation of a cold unmagnetized plasma) and therefore with the refractive index, it has the additional advantage that almost no model assumptions have to be adopted with respect to the plasma. Some exploratory work has been done on the application of microwave interferometry to atmospheric pressure plasmas [18-22]. A microwave absorption system operating at 9.7 GHz was used to determine the electron number density profile of a helium plasma at atmospheric pressure [18]. The electron-neutral collision frequency at one atmosphere pressure is in the order of terahertz, far above the tens of GHz frequency of the microwave signal normally used as an active probing signal for microwave diagnostics. This rules out conventional microwave interferometry as a diagnostic tool for atmospheric pressure plasma. This microwave diagnostic method will yield both the electron number density and collision frequency of atmospheric pressure plasma from measured quantities [23,24].

In previous chapters, the experimental setup and measurements of a fluorescent lamp plasma have been presented. We extend this diagnostic method to time-averaged measurements of the One Atmosphere Uniform Glow Discharge Plasma (OAUGDP^{TM}) operating in air. The broader goal is to develop a new plasma diagnostic method for atmospheric plasma characterization as well as process monitoring and control of atmospheric pressure glow discharges.

Using the experimental setup discussed in Chapter 4, the time-averaged attenuation and phase shift of a microwave signal through OAUGDP^{TM} plasma can also be measured. These measured quantities are related to the electron density and collision frequency, shown in (5.1.1) and (5.1.2), the derivation of which is given in Chapter 3.

$$\alpha(\mathrm{dB}) = 10\log_{10}\left\{\left(\frac{E}{E_0}\right)^2\right\} = 10\log_{10}\left(e^{-\frac{2d}{\delta}}\right)$$
$$= 10\log_{10}\left(e^{-\frac{2d\omega}{c}\chi}\right) = f(n_e, \nu_c, \omega, d) \qquad (5.1.1)$$

$$\Delta\phi(\text{degree}) = \phi - \phi_f = \left(\frac{\omega}{c}\mu - \frac{2\pi}{\lambda}\right)d = g\left(n_e, \nu_c, \omega, d\right) \tag{5.1.2}$$

5.2 Measurement of a Surface OAUGDP^{TM} Generated by a Flat Panel

The surface OAUGDP^{TM} plasma is generated in air on a dielectric panel, on which a series of parallel, plasma-generating electrodes are located. A characteristic RF plasma driving frequency is 3–10 KHz, and the operating voltage is 3 – 6 kV (RMS) [25]. A flat panel OAUGDP^{TM} reactor is shown in Figure 5.2.1. The plasma is generated in air at 760 Torr pressure on the surface of a 25 cm × 25 cm dielectric panel, the thickness of which is 0.6 mm. Parallel strip copper electrodes are placed on the upper surface of the panel. The width of each strip electrode is 0.5 mm and the center-to-center spacing between electrodes is 3 mm. All parallel strip electrodes are connected at the end by a 2-mm-wide bus electrode. The bottom surface of the panel is covered by a copper sheet, which serves as the bottom electrode, as well as a microwave reflector for the experimental system. We power the upper and bottom electrodes to generate a uniform glow discharge on the upper surface. The threshold voltage to generate the plasma is 3 KV (RMS). The power supply generates a RF signal with frequency up to 12 KHz and voltage up to10 KV (RMS). The impedance matching network consists of a group of capacitors and inductors, and helps to optimize and make uniform the glow discharge. By adjusting a resistance in the impedance matching network, the voltage fed to the panel can be maintained at the same level at different driving frequencies from 2.5 KHz to 12 KHz. Therefore a flat surface OAUGDP^{TM} plasma can be generated at different RF driving frequencies. The frequency effect on the microwave-plasma interaction will be studied.

Figure 5.2.2 shows the panel when plasma is on and off. The thickness of the surface OAUGDP^{TM} was estimated visually. Paper sheets were stacked beside the blue-color plasma until the thickness of paper was the same as the thickness of plasma, judging by eye. The plasma thickness is estimated to be about 0.3 mm.

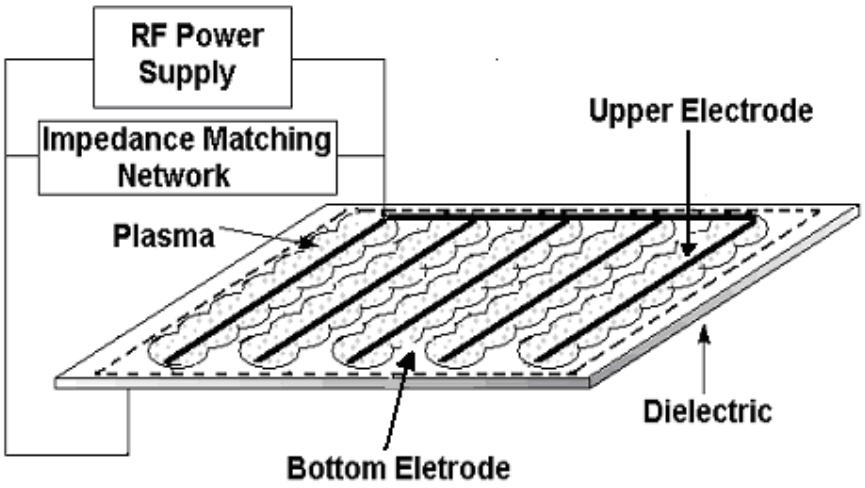

Figure 5.2.1: Flat panel OAUGDP^{TM} reactor.

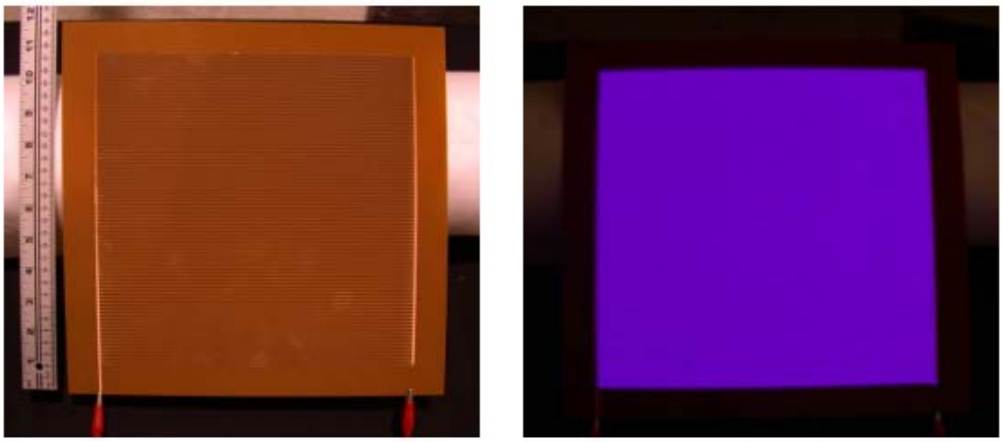

a) Plasma off b) Plasma on

Figure 5.2.2: Plasma panel.

a) Not energized, b) Energized at 8.5 KHz and 5 KV (rms).

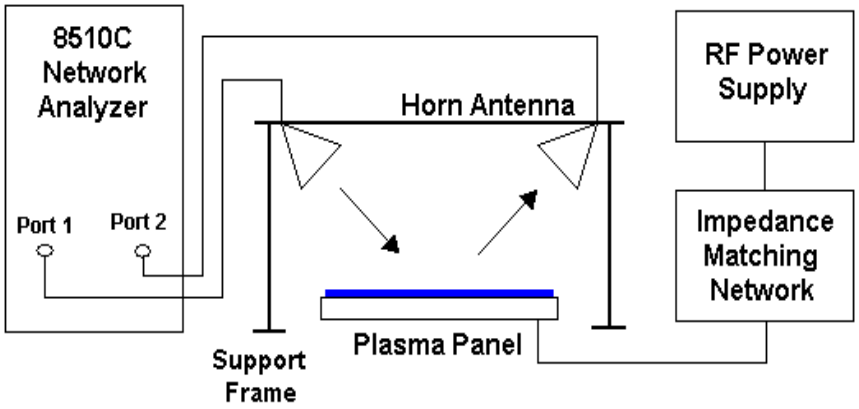

Figure 5.2.3: Measurement system.

The measurement system is illustrated in Figure 5.2.3. It includes the plasma reactor, the power supply, the impedance matching network, the HP 8510C network analyzer system, and the microwave horns. Two 20 dB standard gain horns are mounted on a supporting frame so that the horn position may be adjusted and the incident angle can range from 0 degrees to 60 degrees. Only one horn antenna is used for the 0^0 incident angle, and the only horn serves as both transmitter and receiver. The 3 dB beam width of the horns is 18.8° in E plane and 18.9° in the H plane. Since the panel dimension is 25 cm x 25 cm, the distance the horns can be placed from the panel should be less than 90 cm. Also, in order to make the horns operate in the far field mode, the distance from the panel should not be less than 30 cm for a 15 GHz incident microwave signal. The horns are connected to the network analyzer by a 1.5 m flexible microwave coaxial cable. Figure 5.2.4 shows a photograph of our experimental setup. The incident angle is 0^0, so only one horn antenna is used in Figure 5.2.4.

In the experiment, the microwave signal is input by the network analyzer and penetrates the plasma layer. The copper sheet on the bottom surface of the dielectric panel then reflects the incident microwave signal. The network analyzer detects the reflected signal and analyzes the attenuation and phase shift information. Figure 5.2.5 shows the alignment of the microwave horns with the dielectric panel and the

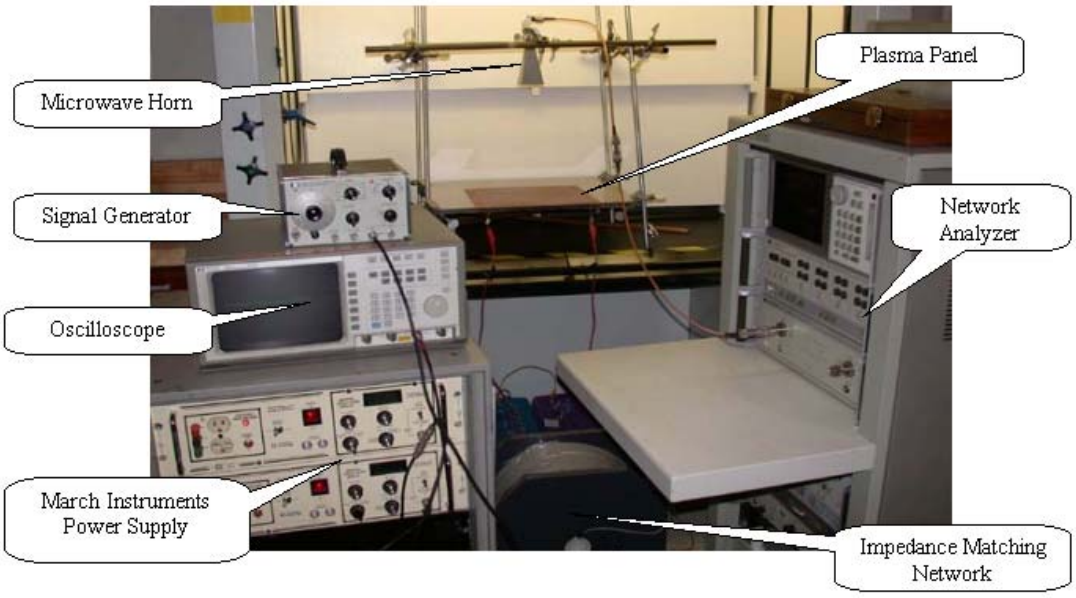

Figure 5.2.4: Photograph of experimental setup.

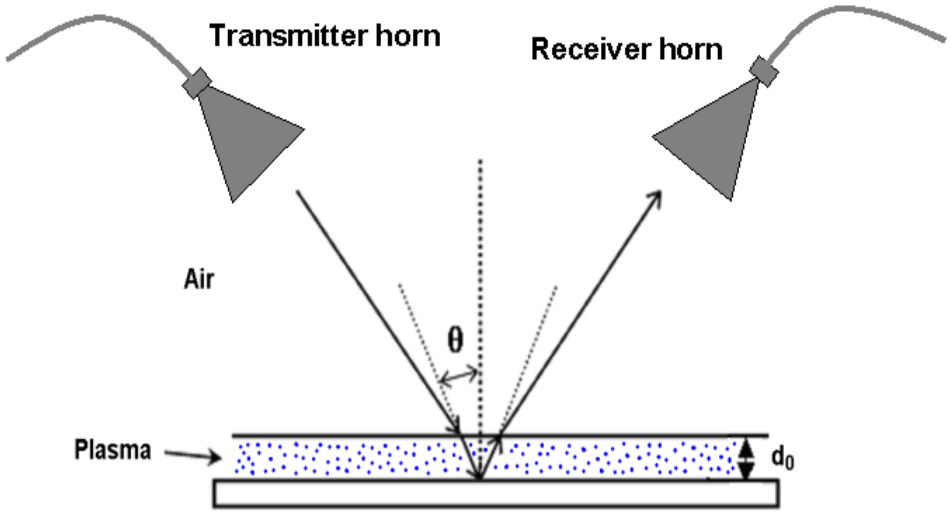

Figure 5.2.5: Microwave signal penetrating flat panel plasma.

microwave signal path. The actual length of the signal path through plasma layer should vary with the incident angle. Since the thickness of the plasma layer and the dielectric panel is less than 1 mm, the refraction effect when microwaves propagate from one medium to another should be negligible when we later consider the length of the signal path.

The flat panel OAUGDP^{TM} measurement is time-averaged. By adjusting the impedance matching network, the plasma RF driving frequency and voltage, and the plasma panel structure, we found the optimum plasma-microwave interaction condition that will maximize the attenuation through the plasma, and produce the highest signal-to-noise ratio. Since the plasma on the flat panel is only about 0.3 mm thick, the potential difficulty we anticipate is that the measured attenuation and time delay might be as low as the network analyzer measurement resolution. Some preliminary data have been acquired in the configuration of Figure 5.2.5.

Figure 5.2.6 shows the measured attenuation from the OAUGDP^{TM} plasma at different driving frequencies, which range from 2.5 KHz to 12 KHz. The voltage was maintained at 5 KV (RMS) at all frequencies. The measured data reveal that the phase change of the microwave signal is too small to be detected by the network analyzer. When the phase change was simulated numerically we did not find a phase change due to plasma that was above the network analyzer threshold of 0.1^0. From Figure 5.2.6, we can see that for the same plasma panel, with the same driving voltage, there is no experimentally measured attenuation below 7 KHz and above 10 KHz. We hypothesize that between 7 KHz and 10 KHz, the plasma generated on the upper surface of the panel operates in an optimum state, in which the microwave interaction with the plasma is observable above the network analyzer noise level, 0.01 dB and damps effectively. Maximum attenuation occurs from 8 KHz to 9 KHz.

After measuring the attenuation and attempting to measure the phase shift at different plasma RF driving frequencies, we operated the plasma only at the optimum frequency of 8.5 KHz. Measurements are made at 3 incident angles, which are 0 degrees, 30 degrees and 60 degrees. The distance between horns and plasma panel is 40 cm, so that plasma is in the far field. For every incident angle, measurements are made at two plasma driving voltages, 4 KV (RMS) and 5 KV (RMS). The measured data are shown in Figure 5.2.7, which shows that the plasma generated by a higher

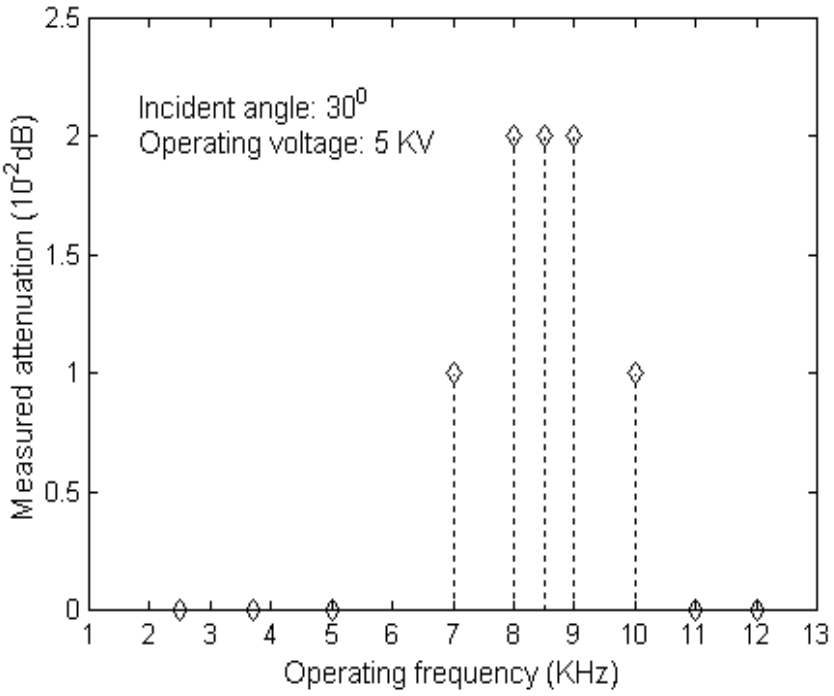

Figure 5.2.6: Attenuation versus RF frequency.

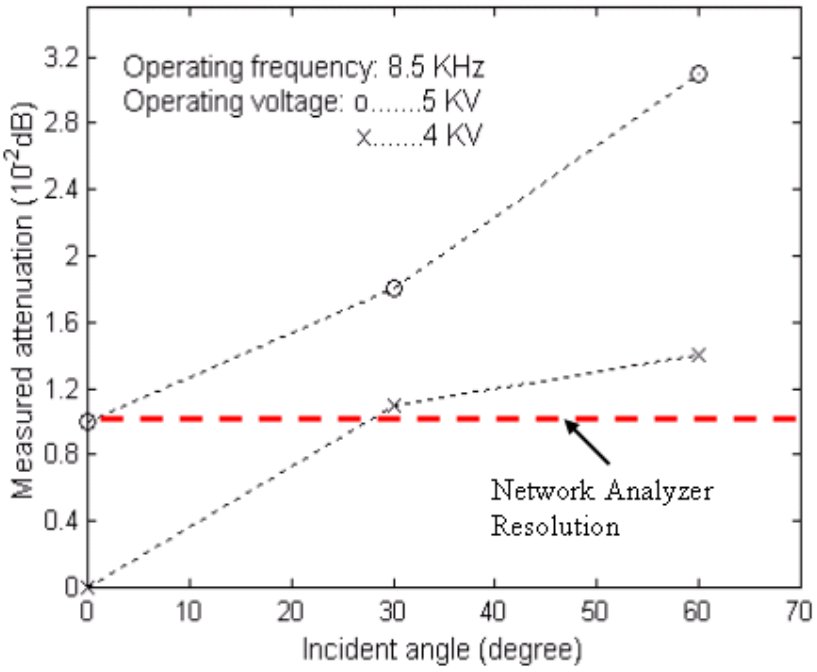

Figure 5.2.7: Attenuation versus RMS voltage.

voltage induces a higher attenuation. The phase shift should have the same trend, but the network analyzer system could not detect the change phase in angle.

The procedure used to obtain the electron density and collision frequency from the attenuation and phase shift information has been discussed in Chapter 2. Equation (5.1.1) and (5.1.2) also describe the relationship between the measured and plasma parameters. In this experiment, the incident microwave is 15 GHz and the plasma thickness is estimated to be 0.3 mm. For an incident angle of 60^0, the effective plasma thickness, which is the microwave signal path through plasma, is estimated to be $2 \times 0.3/\cos 60^0$ mm. Given the collision frequency range of 1.1×10^{12} -- 4.9×10^{12} collision/s, the attenuation defined by (5.1.1) is plotted as a function of electron number density in Figure 5.2.8, and the phase shift is plotted in Figure 5.2.9. Since only the attenuation can be measured, there is not enough input information for Equation (5.1.1) and (5.1.2) to be solved for both the electron number density and collision frequency. Only an operating region of electron number density can be given, shown in Figure 5.2.8. The data in Table 5.2.1 is for the plasma panel operating at 8.5 KHz and 4 KV. The data in Table 5.2.2 are for the plasma panel operating at 8.5 KHz and 5 KV. The electron number density is estimated within the collision frequency limit of 466×10^9 -- 4.1×10^{12} collision/s.

5.3 Investigation on Parallel Plate OAUGDP^{TM} Plasma

The parallel plate plasma reactor configuration is widely used in such industrial applications as microelectronic etching and surface treatment. Our parallel plate OAUGDP^{TM} reactor operates in air at the RF plasma driving frequency of 3-10 KHz. Compared to the flat panel plasma, there is a much larger volume of plasma generated by the parallel plate reactor. The goal is to acquire more promising attenuation and phase shift data, with a higher signal-to-noise ratio than that of the flat panel. With both measured attenuation and time delay information, we can derive both electron number density and collision frequency. First, the experiment will concentrate on time-averaged measurements. Once these yield useful insights into the electron number density and collision frequency of the plasma, the experiment will be extended to time-resolved measurements.

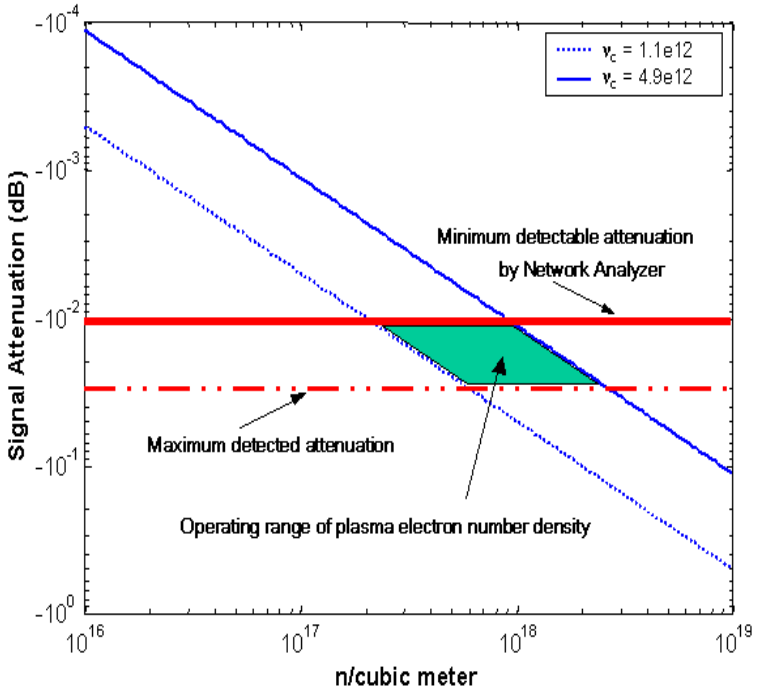

Figure 5.2.8: Attenuation of panel plasma as a function of electron number density.

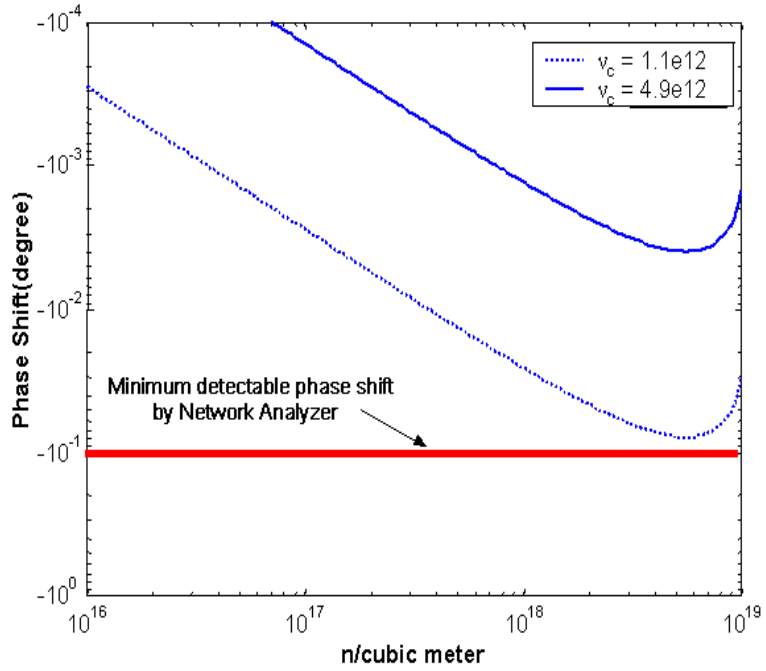

Figure 5.2.9: Phase shift of panel plasma as a function of electron number density.

Table 5.2.1: f = 8.5 KHz, V = 4 KV, $\nu_c = 466x10^9 – 4.1x10^{12}$ collision/s.

Incident angle	0^0	30^0	60^0
Measured Attention (dB)	0.010	0.018	0.031
Signal path (mm)	0.3	0.35	0.6
Electron density (cm^{-3})	$4.0x10^{11}$ ---- $1.8x10^{12}$	$6.2x10^{11}$ ---- $2.7x10^{12}$	$6.2x10^{11}$ ---- $2.7x10^{12}$

Table 5.2.2: f = 8.5 KHz, V = 5 KV, $\nu_c = 466x10^9 – 4.1x10^{12}$ collision/s.

Incident angle	0^0	30^0	60^0
Measured Attention (dB)	0	0.011	0.014
Signal path (mm)	0.3	0.35	0.6
Electron density (cm^{-3})	----	$3.8x10^{11}$ --- $1.7x10^{12}$	$2.8x10^{11}$--- $1.2x10^{12}$

The UT Plasma Sciences Laboratory has developed Mod VI and Mod VII parallel plate reactors. The Mod VI reactor has circular electrodes, the diameter of which is 16 cm. The Mod VI reactor can generate a uniform glow discharge with a maximum electrode gap distance of 4 mm.

From an electromagnetic point of view, the electrodes of a parallel plate reactor can be modeled as a parallel plate waveguide. A cutoff frequency exists for waves propagating in such a waveguide. The cutoff frequency is related to the wave propagation mode and the waveguide dimensions. However, the cutoff frequency for the TEM mode is 0, so a plane electromagnetic wave can propagate through the parallel plate waveguide regardless of the wave frequency and the waveguide dimensions. When a microwave signal in the mode propagates through the plasma generated between such plates, there will exist an attenuation and phase shift, since the plasma is a lossy medium. In future experiments, horn antennas will be used to transmit a TEM mode microwave signal through the OAUGDP^{TM} plasma generated in a parallel plate reactor. The time-dependent attenuation and phase shift will be measured by an experimental arrangement similar to that used for the fluorescent lamp plasma measurements. Figure 5.3.1 illustrates the alignment of horns for the parallel plate reactor.

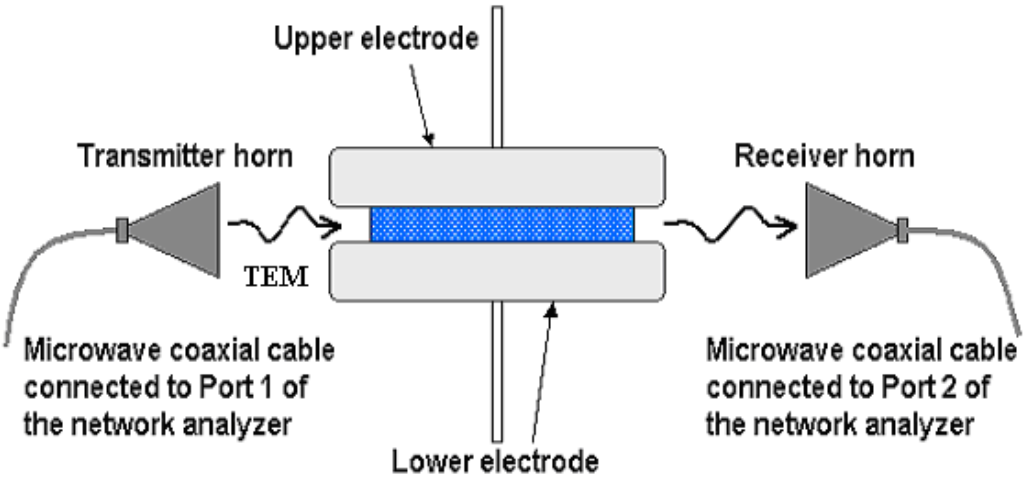

Figure 5.3.1: Alignment of horns for parallel-plate reactor.

As discussed above, time-resolved measurements on the parallel plate plasma will be studied. Compared to the time-resolved measurement on fluorescent lamp plasma, such measurements on the OAUGDP^{TM} plasma are more difficult because of the higher plasma driving frequency. When the HP 8510C network analyzer is configured to make time-resolved measurements, the maximum sampling rate is 100 Hz, while the OAUGDP^{TM} plasma driving frequency is 3-10 KHz. Assuming the maximum sampling rate is applied, a 100 Hz pulsed signal will be synchronized with the plasma driving frequency, for example 2 KHz, and trigger network analyzer measurement. Only one measurement point occurs in every 20 plasma cycles. Furthermore, there is a time delay after the network analyzer receives an externally triggering pulsed signal. As is discussed in Chapter 4, the time delay is not a constant and can range from 80 μs to 1 ms depending on the network analyzer system configuration. Since the typical plasma cycle of OAUGDP^{TM} is only 200 μs (5 KHz), it will be extremely difficult to make accurate time-resolved measurements without a major re-design of the sampling circuit.

Chapter 6
Future Work and Conclusions

6.1 Future Work on Plasma Drift Velocity Measurement by Doppler Effect

One future objective is to measure the Doppler shift of the reflected microwave signal. The plasma panel shown in Figure 6.1.1would have asymmetric electrodes on the upper and lower surface of the panel, which can impart a convective velocity to the plasma and boundary air layer in the range of 5 to 10 m/s due to paraelectric effects [27, 28, 29]. The neutral flow generated on the panel surface will induce a Doppler effect to the microwave signal if the signal reflects from the flowing plasma. The Doppler effect can be detected by comparing the incident microwave signal and reflected microwave signal using the network analyzer.

Figure 6.1.2 shows the Doppler effect measurement setup. The Doppler shift is derived as

$$f_D = \frac{-2 f_0 v \cos \theta}{c}, \tag{6.1.1}$$

where f_D is the Doppler shift in Hertz, f_0 is the transmitted frequency, v is the plasma convective velocity, c is the free space light velocity, and θ is the incident angle. For a convective velocity of 5 m/s, a microwave incident angle of 30 degrees and the flow direction indicated in Figure 6.1.1, the Doppler shift is 433 Hz. The potential difficulty of such a measurement is that a microwave source and detector with high frequency resolution are needed to measure such a relatively small frequency shift. First it requires a high-resolution microwave source, which can generate a microwave signal with a highly precise frequency. The UT Plasma Sciences Laboratory upgraded the microwave source of the network analyzer, which can synthesize a microwave signal with 1 Hz frequency resolution. Second, it requires the network analyzer to detect two signals with a frequency shift as small as 433 Hz. Since the 8510C vector network analyzer does not have the capability to detect such a small frequency shift, a high frequency resolution spectrum analyzer is required to make the measurement. If the Doppler shift of reflected microwave signal can be measured, the convective flow velocity can be calculated from Equation (6.1.1). The flow velocity derived from a Doppler shift will be compared to the flow velocity measured by a Pitot probe system [27, 28].

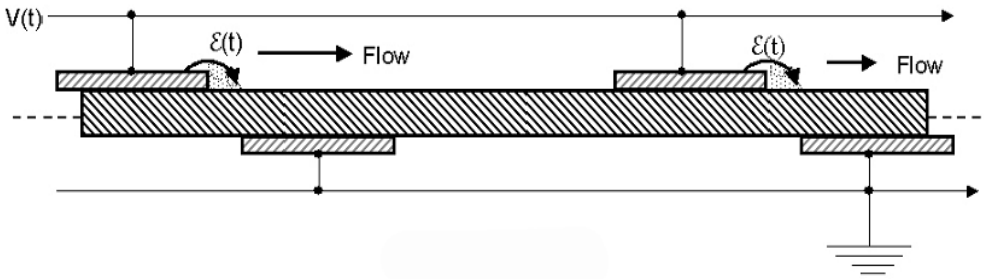

Figure 6.1.1: Paraelectric panel.

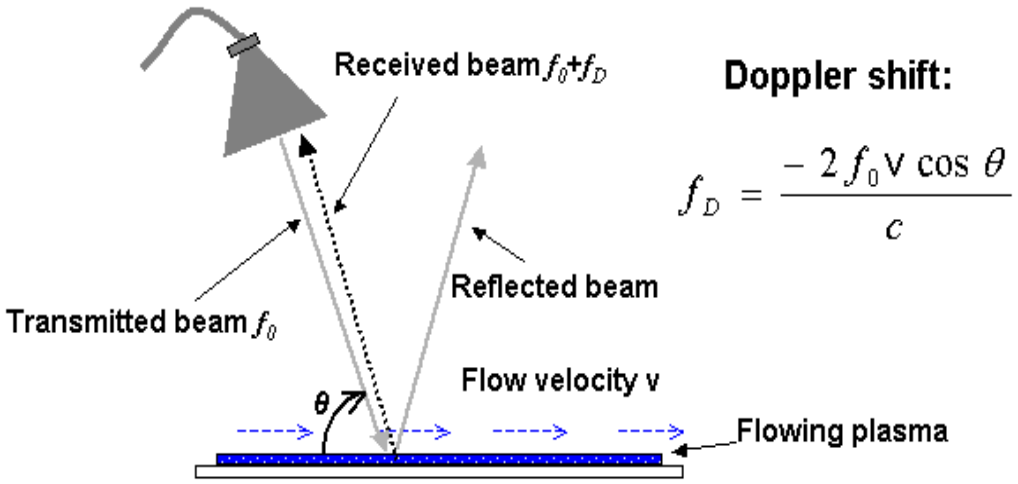

Figure 6.1.2: Proposed experimental setup for Doppler effect measurement.

6.2 Conclusion

A microwave-based plasma diagnostic method has been implemented to yield theoretically well-founded measurements of the time-resolved electron number density and electron collision frequency in glow discharge plasmas. The variation of the attenuation and phase shift of a fluorescent lamp tube plasma during one plasma cycle, and data on the electron number density and collision frequency have been demonstrated. The characteristics of plasma generated by a mercury-based fluorescent lamp and a "mercury-free" fluorescent lamp were compared. This information may help to understand and improve the performance of fluorescent lamps. While the measurement of an OAUGDP^{TM} surface plasma (0.3 m thick) is not as satisfactory as that of the fluorescent lamp plasma, narrow limits on the electron number density and collision frequency have been obtained for a flat panel in air, the OAUGDP^{TM} of which is only 0.3 mm in thickness.

The attenuation and the phase shift are determined from the measurement of the transmission coefficient S_{21}. Several errors should be taken into account: a) instrument-related errors; b) multiple reflections within the light tube; c) multiple path transmission; d) violation of the far-field condition; e) surface and volume scattering; f) divergence due to refraction; g) aperture diffraction. Among these errors, the instrument-related errors can be quantitized and minimized by the network analyzer system calibration. After calibrating the network analyzer and time gating the measured data, the noise level can be decreased to as low as ±0.01 dB for amplitude and ±0.10 degree for phase measurement. The errors due to multiple reflections and multiple path transmission can be filtered out by applying the time-domain gating feature of the network analyzer. Other sources of error are more difficult to calculate rigorously. Rather than attempting to quantify them, we take appropriate precautions to minimize their respective effects. Those precautions can be: 1) the alignment the antennas must be accomplished by peaking the receiving signal level in transmission measurement; 2) the horns are separated far enough from each other so that plasma is in the far field region; 3) the plasma under test must be positioned at the place where the wave can be considered a plane (TEM) wave; 4) using metal limiters to minimize the cylindrical refractive effect.

The measurement system utilizes the capabilities of a network analyzer as a stable microwave source and highly sensitive receiver and detector. As is discussed, some remarkable features of the network analyzer are employed to make simple and accurate transmission measurements. First, the time gating feature is used for isolating the target signal, which passes through the plasma, from those interference signals caused by the vibration and multipath effect. Only a 15 GHz microwave signal is considered in the experiment, but in order to effectively time gate the signal, the frequency must be swept from 14.5 GHz to 15.5 GHz and the time gating span must be carefully selected. Second, the external trigger feature is employed to make time-resolved measurements. The microwave source of the network analyzer has been upgraded to acquire the unique external triggering feature. The time-resolved experimental setup works well for the fluorescent lamp plasma. When it comes to OAUGDP^{TM} plasma, the conclusion of this study is that the time-resolved measurement for OAUGDP^{TM} plasma cannot be done with the current network analyzer configuration. The 8510C network analyzer provides 100 Hz sampling speed for time-resolved measurement while the OAUGDP^{TM} plasma is driven by a 2 – 10 KHz signal. Only time-averaged measurements can be made for the OAUGDP^{TM} with the current system.

The final result of this study is that the proposed microwave diagnostic technique is a technically viable method to measure the electron number density and collision frequency of glow discharge plasma, both at low pressure and atmospheric pressure plasma. The method of deriving plasma parameters from measured quantities is robust, flexible and reliable. If the expensive network analyzer can be replaced by a simpler and less expensive microwave system, this technique will have many applications in industry and plasma research laboratories.

References

[1] J. R. Roth, *Industrial Plasma Engineering: Volume I, Principles,* Institute of Physics Publishing, Bristol and Philadelphia 1995.

[2] M A Heald and C B Wharton, *Plasma Diagnostics with Microwaves,* Rober E. Krieger Publishing Company 1978.

[3] Lawrence J. Overzet, and B. Hopkins, "Comparison of electron-density measurements made using a Langmuir probe and microwave interferometer in the Gaseous Electronics Conference reference reactor," *J. Appl. Phys.* 74 (7), October 1993.

[4] Shawn G. Ohler, Brian E. Gilchrist, and Alec D. Gallimore, "Nonintrusive electron number density measurements in the plume of a 1 KW arcjet using a modern microwave interferometer," *IEEE Transaction on Plasma Science* 23 (3), June 1995.

[5] Ch Lukas, M. Muller, V. Schulz-von der Gathen, and H.F. Dobele, "Spatially resolved electron number density distribution in an RF excited parallel plate plasma reactor by 1 mm microwave interferometry," *Plasma Sources Sci. Technol.* 8 (94-88), 1999.

[6] B.E. Gilchrist, S.G. Ohler, and A.D. Gallimore, "Flexible microwave system to measure the electron number density and quantify the communication impact of electric thruster plasma plumes," *Rev. Sci. Instrum*. 68 (2), February 1997.

[7] K.R. Stalder, R.J. Vidmar, and D.J. Eckstrom, "Observations of strong microwave absorption in collisional plasmas with gradual density gradients," *J. Appl. Phys*. 72 (11), December 1992.

[8] A. Singh, W.W. Destler, P. Catravas, and J. Rodgers, "Experimental study of interaction of microwaves with a nonmagnetized pulsed-plasma column," *J. Appl. Phys*. 72 (4), September 1992.

[9.] R.B. Gadri, "One atmosphere glow discharge structure revealed by computer modeling," *IEEE Trans. on Plasma Sci.* Vol 27, Feb. 1999.

[10.] R.H. Freeman, and J.A. Roberts, "Electron collision frequency observations in H_2, D_2, N_2O, CO_2 and Argon at pressures of 0.4-2 torr," *Plasma Phys.* Vol.16(377), 1974.

[11.] P. Baille, etc., "Effective collision frequency of electrons in noble gases," *J. Phys. B: At Mol. Phys.* 14(1485-1495), 1981.

[12.] Graeme G. Lister, "Collisional and radiative processes in fluorescent lamps," *Phys. of Plasma,* 10 (5), May 2003.

[13.] W. McColl, C. Brooks, and M.L. Brake, "Electron density and collision frequency of microwave-resonant-cavity-produced discharges," *J. Appl. Phys.* 74 (6), September 1993.

[14.] C.C. Motta, A.D. Fonseca, G.H. Gomes, and H.S. Maciel, "Electron number density and collision frequency measurements in a microwave surface wave discharge," Conference record, IEEE Conference of Pulsed Power Plasma Science, Las Vegas, NV, June 2001.

[15.] L.P. Bakker, and G.M.W. Kroesen, "Thomson scattering in a low-pressure argon mercury positive column," *J. Appl. Phys*. 88 (7), October 2000.

[16.] S. Y. Moon, W Choe, Y. S. Hwang, and J. J. Choi, "Determination of the two-dimentional distribution of plasma parameters in an atomospheric microwave plasma," IEEE International Conference on Plasma Science, 2P06, Banff, Alberta, Canada, May 2002.

[17.] F Leipold, R. H. Stark, A. El-Habachi and K. H Schoenbach, "Electron density measurements in an atmospheric pressure air plasma by means of infrared heterodyne interferometry," *J. Phys. D: Appl. Phys.* Vol. 33, No.18, pp. 2268-2273, September 2000.

[18.] K. R. Stalder, R. J. Vidmar, and D. J. Eckstrom, "Observations of strong microwave absorption in collisional plasma with gradual density gradients," *J. Appl. Phys.* Vol. 72, pp. 5089-5094, Dec. 1992.

[19.] S. G. Ohler, B. E. Gilchrist, and A. D. Gallimore, "Nonintrusive electron number density measurements in the plume of a 1 KW arcjet using a modern microwave interferometer," *IEEE Trans. on Plasma Science*, Vol. 23, Issue 3, pp 428-435, June 1995.

[20.] K. R. Stalder, "Measurement of electron densities and collision frequencies using microwaves," IEEE International Conference on Plasma Science, 6P33, Raleigh, NC., June 1998.

[21.] C.H. Kruger, E.E. Kunhardt, C.O. Laux, and K.H. Schoenbach, "Measurement of electron densities in weakly ionized atomopheric pressure air," IEEE International Conference on Plasma Science, 6P50, Raleigh, NC., June 1998.

[22.] F. Leipold, and K. H. Schoenbach, "Electron density and electron temperature in pulsed atmospheric pressure air plasma," IEEE Internaltional Conference on Plasma Science, 2P03, Banff, Alberta, Canada, June 2002.

[23.] Howlader M., Yang Y., and Roth J. R., "Time averaged electron number density measurement of a One Atmosphere Uniform Glow Discharge Plasma (OAUGDP^{TM}) by Absorption of Microwave Radiation," Paper 5P-29, Proceedings of the 29th IEEE International Conference on Plasma Science, Banff, Alberta, Canada, May 2002.

[24.] Howlader M., Yang Y. and Roth J. R., "Measurement of electron number density and collision frequency in a One Atmosphere Uniform Glow Discharge Plasma using a microwave network analyzer," Paper GTP-055, 55th APS Gaseous Electronic Conference, Minneapolis, Minnesota, Oct. 2002.

[25.] Roth J. R., Tsai P. P., Liu C., Laroussi M. and Spence P. D., "One Atmosphere Uniform Glow Discharge Plasma", U. S. Patent #5,414,324, Issued May 9, 1995.

[26.] Chen Z. and Roth J. R., "Impedance Matching for One Atmosphere Uniform Glow Discharge Plasma (OAUGDP) Reactors", Paper P2H-15, Proceedings of the 28th IEEE International Conference on Plasma Science, Las Vegas, NV, June 2001.

[27.] J. R. Roth, "Aerodynamic Flow Acceleration Using Paraelectric and Peristaltic Electrohydrodynamic (EHD) Effects of a One Atmosphere Uniform Glow Discharge Plasma," *Physics of Plasmas*, Vol. 10, No. 5, 2003.

[28.] Roth, J. R., Sin H., Mohan R.C.M. and Wilkinson S. P., "Flow Re-attachment and Acceleration by Paraelectric and Peristaltic Electrohydrodynamic Effects", Paper AIAA 2003 - 531, Proc. 41st Aerospace Sciences Meeting and Exhibit, Reno, NV, January, 2003.

[29.] Sherman D. M., Wilkinson S. P., and Roth J. R., “Paraelectric Gas Flow Accelerator”, U. S. Patent # 6,200,539 B1, Issued March 13, 2001.

Vita

Yunqiang Yang was born on October 22, 1978 in Shanghang, Fujian, People's Republic of China. He received his Bachelor of Science degree in Electrical Engineering from Zhejiang University (Hangzhou, Zhejiang, China) in July 2001. He began the graduate study of the Master of Science degree in Electrical Engineering from August 2001 at University of Tennessee, Knoxville. He has served as a Graduate Research Assistant at the UT Plasma Sciences Lab thereafter. His research work involves the development of a microwave diagnostic method for atmospheric pressure plasmas. He is currently an IEEE student member.